OBSERVATION

Limb-Girdle Muscular Dystrophy Due to Emerin Gene Mutations

Shigehisa Ura, MD; Yukiko K. Hayashi, MD, PhD; Kanako Goto, MS; Mina Nolasco Astejada, MD; Terumi Murakami, MD; Masako Nagato, MD; Shigeru Ohta, MD; Yasuhisa Daimon, MD; Hidehiro Takekawa, MD, PhD; Koichi Hirata, MD, PhD; Ikuya Nonaka, MD, PhD; Satoru Noguchi, PhD; Ichizo Nishino, MD, PhD

Background: Emery-Dreifuss muscular dystrophy, caused by *EMD* gene mutations, is characterized by humeroperoneal muscular dystrophy, joint contractures, and conduction defects and is often associated with sudden cardiac death, even without prior cardiac symptoms.

Objective: To describe the clinical and molecular features of 2 patients with limb-girdle muscular dystrophy with mutations in *EMD*.

Design: Case reports.

Setting: Academic research.

Patients: Two male patients manifested proximal dominant muscle involvement, with minimal or no joint and cardiac involvement.

Main Outcome Measures: Muscle biopsy and mutation analysis results.

Results: Immunohistochemistry revealed an absence of emerin staining in muscle biopsy specimens. Mutation analysis identified nonsense mutations in *EMD*.

Conclusions: Mutations in *EMD* may indicate a limb-girdle muscular dystrophy phenotype. Identification of emerin deficiency among patients with limb-girdle muscular dystrophy is essential to prevent cardiac catastrophe.

Arch Neurol. 2007;64(7):1038-1041

Author Affiliations: Department of Neuromuscular Research, National Institute of Neuroscience, National Center of Neurology and Psychiatry, Tokyo (Drs Ura, Hayashi, Astejada, Murakami, Nonaka, Noguchi, and Nishino and Ms Goto); Department of Pediatrics, Tenri Hospital, Nara (Drs Nagato and Ohta); and Department of Neurology, Dokkyo Medical University, Tochigi (Drs Daimon, Takekawa, and Hirata), Japan.

EMERY-DREIFUSS MUSCULAR dystrophy (EDMD) is a rare muscular dystrophy clinically characterized as a triad of (1) slowly progressive humeroperoneal muscular dystrophy; (2) early joint contractures of Achilles tendons, elbows, and hind neck, and (3) cardiomyopathy with conduction defects.[1] The X-linked form of EDMD is caused by mutations in the emerin gene (*EMD*) or in *STA* on Xq28,[2] whereas autosomal dominant and rare recessive forms of EDMD are caused by mutations in the lamin A/C gene (*LMNA*) on 1q21.[3] *EMD* is composed of 6 small exons that encode emerin, a 34-kDa inner nuclear membrane protein.[3,4] Immunohistochemical analysis is valuable for the diagnosis of the X-linked form of EDMD because most patients show a lack of emerin staining at the nuclear membrane of skin, leukocytes, and skeletal and cardiac muscles.[5-7] *LMNA* encodes lamin A and C, which are major components of nuclear lamina. Emerin and lamin A/C are nuclear envelope proteins, and clinical features of the X-linked form of EDMD and autosomal dominant EDMD are similar and indistinguishable. However, mutations in *LMNA* are known to be associated with several other disorders collectively known as *laminopathies*, including limb-girdle muscular dystrophy (LGMD) type 1B, which is characterized by proximal dominant muscular dystrophy with atrioventricular conduction disturbance.[8] To exclude *EMD* mutations in patients with LGMD, we examined emerin expression in muscle biopsy specimens and performed genetic screening.

METHODS

MUSCLE BIOPSY SPECIMENS

All clinical materials used in this study were obtained for diagnostic purposes following informed consent. Skeletal muscle biopsy specimens were flash frozen in isopentane chilled with liquid nitrogen. A panel of histochemical staining, including hematoxylin-eosin and modified Gomori trichrome, was performed to obtain the pathological diagnosis. Immunohistochemical and immunoblotting analyses

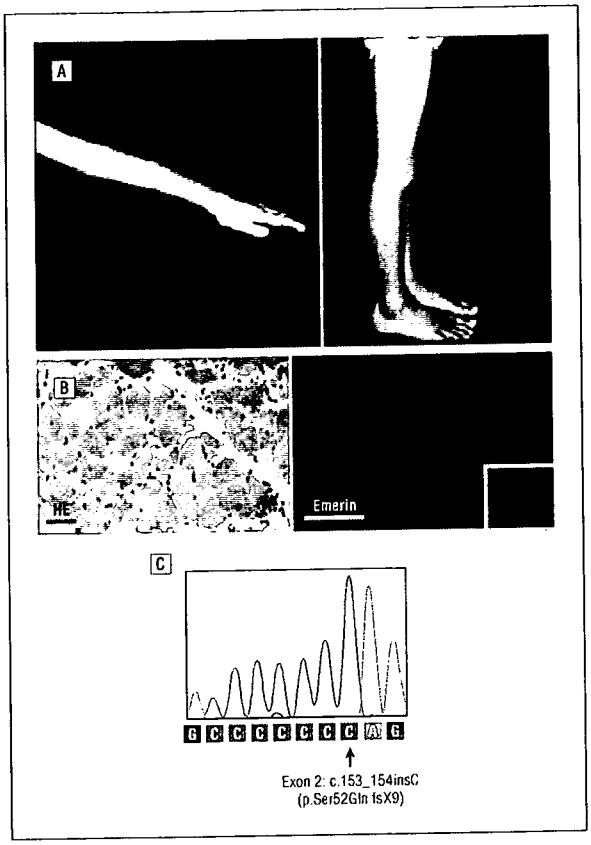

Figure 1. Patient 1. A, A 9-year-old boy had proximal muscle atrophy without joint contractures. B, Hematoxylin-eosin (HE) staining and emerin immunoreaction (Emerin) of skeletal muscle biopsy specimen. The HE staining shows fiber-size variation, regenerating fibers, and fibers with internalized nuclei. Immunoreaction of emerin is absent at the nuclear membrane. The bar indicates 50 µm. Inset, Emerin staining of control muscle is shown. C, Mutation analysis revealed a 1–base pair insertion at c.154 in exon 2.

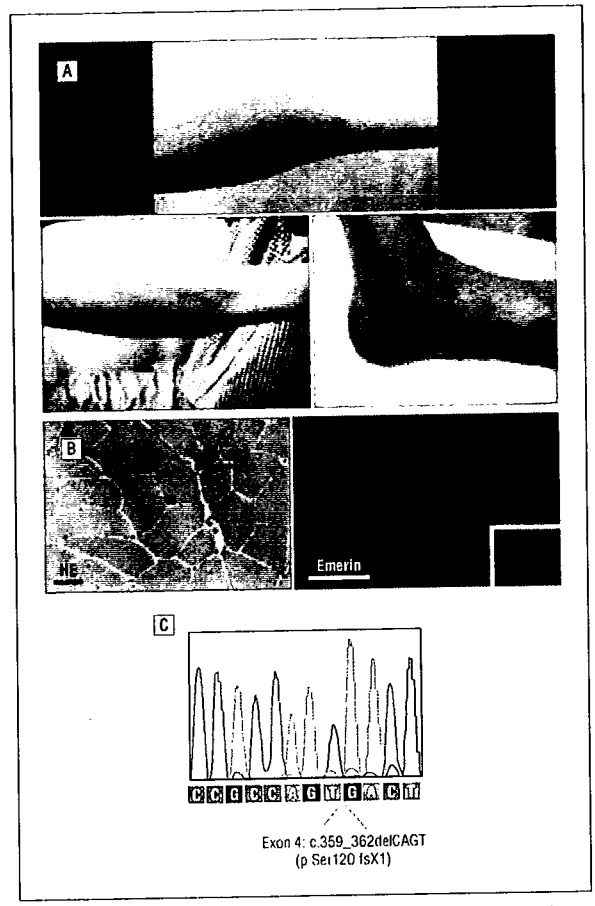

Figure 2. Patient 2. A, A 50-year-old man had proximal dominant muscle atrophy of the limbs with minimal joint contractures at the right elbow and Achilles tendon. B. Hematoxylin-eosin (HE) staining and emerin immunoreaction (Emerin) of muscle biopsy specimen. The HE staining shows fiber-size variation, regenerating fibers, and fibers with internalized nuclei. Immunoreaction of emerin is absent at the nuclear membrane. The bar indicates 50 µm. Inset, Emerin staining of control muscle is shown. C, Direct sequence analysis revealed a 4–base pair deletion at c.359-362 in exon 4.

were conducted as previously described.[9] Genomic DNA was extracted from muscle biopsy specimens or from peripheral lymphocytes using standard techniques.

We examined 94 patients who were clinically and pathologically diagnosed as having LGMD. Exclusion of LGMD types 1C, 2A to 2G, 2I, and 2K was performed by immunohistochemical and Western blotting analyses. In detecting emerin in skeletal muscle biopsy specimens, monoclonal antiemerin antibody (Novocastra Laboratories, New Castle upon Tyne, England) was used.

MUTATION ANALYSIS

All 6 exons and their flanking intronic regions of *EMD* were directly sequenced using an automated sequencer (ABI PRISM 3100; PE Applied Biosystems, Foster City, California). Information about the primers used for the sequence analysis is available from the corresponding author. Sequence analysis of *LMNA* was also performed to exclude LGMD type 1B.

RESULTS

Among 94 patients with LGMD of unknown cause, we identified 2 patients with negative immunostaining for emerin in their skeletal muscles (**Figure 1** and **Figure 2**). Mutation analysis of *EMD* revealed a 1–base pair (bp) insertion (c.153_154insC in exon 2) in patient 1 (Figure 1) and a 4-bp deletion (c.359_362delCAGT in exon 4) in patient 2 (Figure 2). Both mutations were predicted to cause premature termination codon and absence of protein expression.

REPORT OF CASES

Patient 1, a 9-year-old boy from nonconsanguineous parents, neither of whom had neuromuscular or cardiac disorders, was initially seen with proximal dominant muscle weakness and atrophy. He had normal developmental milestones, acquiring independent ambulation at age 1 year; however, unsteady gait was noticed at age 4 years. By age 6 years, he developed weakness and atrophy of the proximal muscles of the lower limbs, waddling gait, and lordotic posture. He then needed support in climbing stairs. On physical examination at age 6 years, his calf muscles were not atrophic. Serum creatine kinase levels were elevated to 927 U/L (to convert

to microkatal per liter, multiply by 0.0167) (reference range, <180 U/L). Muscle biopsy was performed on the left biceps brachii, and the biopsy specimen showed moderate fiber size variation, with some regenerating fibers and several fibers with internalized nuclei (Figure 1). Results of dystrophin immunostaining were positive, and he was diagnosed as having LGMD. At age 9 years, he showed Gowers sign, waddling gait, and proximal dominant limb muscle weakness and atrophy. No joint contractures were observed (Figure 1). An electrocardiogram revealed transient sinus arrhythmia, but his echocardiogram was normal.

Patient 2, a 50-year-old man, initially was seen with proximal dominant muscle weakness and atrophy. His father had died of acute myocardial infarction; his mother was alive without symptoms of neuromuscular or cardiac disorders. He was healthy until age 35 years, when he noticed difficulty in going up and down stairs. During this time, he was incidentally found to have hypertension. Muscle weakness was progressive, and he had difficulty raising his arms by age 40 years. At age 49 years, he required support in climbing stairs and had difficulty in buttoning his clothes. Although his electrocardiogram was normal, an echocardiogram demonstrated moderate mitral and tricuspid insufficiency without dilatation of ventricles. Other than his father's death from acute myocardial infarction, his family history was noncontributory. On physical examination, he had waddling gait, Gowers sign, and proximal dominant muscle weakness and atrophy. Only minimal joint contractures of the right elbow, bilateral Achilles tendons, and neck were observed (Figure 2). His serum creatine kinase level was elevated at 417 U/L. An electromyogram showed myopathy. Results of muscle computed tomography revealed proximal dominant muscle atrophy with fatty tissue replacement. A second electrocardiogram demonstrated complete atrioventricular conduction block. A muscle biopsy specimen was obtained from the left rectus femoris and showed marked fiber size variation, scattered regenerating fibers, and fibers with centrally placed nuclei (Figure 2).

COMMENT

Herein, we demonstrate an expanded clinical spectrum associated with *EMD* mutations, from the X-linked EDMD phenotype to the X-linked LGMD phenotype. The differences between EDMD and LGMD relate to the distribution of affected muscles and to the presence of early joint contractures. From childhood, patients with EDMD having an *EMD* or *LMNA* mutation may demonstrate slowly progressive weakness and wasting of humeroperoneal muscles. Early contracture of the elbows, Achilles tendons, and posterior cervical muscles is another characteristic cardinal feature. Mutations in *LMNA* are associated with variable disorders, including EDMD, LGMD type 1B, peripheral neuropathy, progelia syndromes, lipodystrophy syndrome, and cardiomyopathy with conduction defects. Several overlapping clinical conditions are likewise observed, including an intermediate phenotype of EDMD and LGMD type 1B manifesting as proximal limb muscle involvement with early joint contractures. In contrast, mutations in *EMD* have been associated with only the EDMD phenotype.

A previously described 2½-year-old boy had a condition resembling LGMD with contracture of the right ankle joint requiring Achilles tendon lengthening; this patient had an absence of emerin and had a mutation in *EMD*.[10] Both patients described herein demonstrated proximal muscle weakness with minimal or no joint contractures due to mutations in *EMD*. Patient 1 showed proximal muscular dystrophy without joint contractures and demonstrated only minimal cardiac involvement as transient sinus arrhythmia. However, joint contractures and a severe cardiac condition may develop in this patient. Patient 2 had unusual clinical findings manifesting as adult-onset LGMD. Minimal joint contractures were noticed only after careful physical examination at the age of 50 years. A conduction defect was observed during the course of his cardiac follow-up for valvular insufficiency. It remains unclear whether the absence of emerin has a role in the development of valvular insufficiency observed in this patient. The same mutation identified in patient 2 was previously reported in a patient with typical EDMD.[11] Additional unknown factors may cause different clinical phenotypes in patients harboring identical mutations in the same gene.

Based on these findings, mutations in *EMD* may cause the clinical phenotype of LGMD and the overlapping state of LGMD and EDMD, as seen in patients with mutations in *LMNA*. Cardiac involvement is the most important clinical symptom among patients with *EMD* mutations. Lethal conduction defects with cardiomyopathy have been observed not only in male patients but also in female carriers, at an older age compared with male patients.[12] Careful follow-up of cardiac function is essential, including female family members of patients even in the absence of overt clinical signs or the unavailability of genetic information. Diagnosis of emerin deficiency can be easily performed by immunohistochemical analysis using several tissue specimens. Our results demonstrate the importance of identifying emerin deficiency in patients with LGMD to provide prompt cardiac intervention and to avoid unexpected sudden cardiac death.

Accepted for Publication: December 13, 2006.
Correspondence: Yukiko K. Hayashi, MD, PhD, Department of Neuromuscular Research, National Institute of Neuroscience, National Center of Neurology and Psychiatry, 4-1-1 Ogawa-Higashi, Kodaira, Tokyo 187-8502, Japan (hayasi_y@ncnp.go.jp).
Author Contributions: *Study concept and design:* Ura, Hayashi, Ohta, and Nishino. *Acquisition of data:* Ura, Hayashi, Goto, Astejada, Murakami, Nagato, Ohta, Daimon, Takekawa, and Hirata. *Analysis and interpretation of data:* Ura, Hayashi, Nonaka, Noguchi, and Nishino. *Drafting of the manuscript:* Ura, Nagato, Ohta, Daimon, Takekawa, Hirata, and Noguchi. *Critical revision of the manuscript for important intellectual content:* Hayashi, Goto, Astejada, Murakami, Nonaka, and Nishino. *Obtained funding:* Hayashi and Nishino. *Administrative, technical, and material support:* Hayashi, Goto, Nonaka, and Noguchi.

Study supervision: Daimon, Takekawa, Hirata, and Nonaka.

Financial Disclosure: None reported.

Funding/Support: This study was supported in part by grants from the Human Frontier Science Program and by Research on Health Sciences focusing on Drug Innovation from the Japanese Health Sciences Foundation; by Research on Psychiatric and Neurological Diseases and Mental Health of Health and Labor Sciences Research Grants and Research Grant for Nervous and Mental Disorders from the Ministry of Health, Labor, and Welfare; by a Grant-in-Aid for Scientific Research from the Japan Society for the Promotion of Science; and by the Program for Promotion of Fundamental Studies in Health Sciences of the National Institute of Biomedical Innovation.

REFERENCES

1. Emery AE. Emery-Dreifuss muscular dystrophy and other related disorders. *Br Med Bull.* 1989;45(3):772-787.
2. Bione S, Maestrini E, Rivella S, et al. Identification of a novel X-linked gene responsible for Emery-Dreifuss muscular dystrophy. *Nat Genet.* 1994;8(4):323-327.
3. Bonne G, Di Barletta MR, Varnous S, et al. Mutations in the gene encoding lamin A/C cause autosomal dominant Emery-Dreifuss muscular dystrophy. *Nat Genet.* 1999;21(3):285-288.
4. Yorifuji H, Tadano Y, Tsuchiya Y, et al. Emerin deficiency of which causes Emery-Dreifuss muscular dystrophy, is localized at the inner nuclear membrane. *Neurogenetics.* 1997;1(2):135-140.
5. Nagano A, Koga R, Ogawa M, et al. Emerin deficiency at the nuclear membrane in patients with Emery-Dreifuss muscular dystrophy. *Nat Genet.* 1996;12(3):254-259.
6. Manilal S, Sewry CA, Man N, Muntoni F, Morris GE. Diagnosis of X-linked Emery-Dreifuss muscular dystrophy by protein analysis of leucocytes and skin with monoclonal antibodies. *Neuromuscul Disord.* 1997;7(1):63-66.
7. Mora M, Cartegni L, Di Blasi C, et al. X-linked Emery-Dreifuss muscular dystrophy can be diagnosed from skin biopsy or blood sample. *Ann Neurol.* 1997;42(2):249-253.
8. Muchir A, Bonne G, van der Kooi AJ, et al. Identification of mutations in the gene encoding lamins A/C in autosomal dominant limb girdle muscular dystrophy with atrioventricular conduction disturbances (LGMD1B). *Hum Mol Genet.* 2000;9(9):1453-1459.
9. Tagawa K, Ogawa M, Kawabe K, et al. Protein and gene analyses of dysferlinopathy in a large group of Japanese muscular dystrophy patients. *J Neurol Sci.* 2003;211(1-2):23-28.
10. Muntoni F, Lichtarowicz-Krynska EJ, Sewry CA, et al. Early presentation of X-linked Emery-Dreifuss muscular dystrophy resembling limb-girdle muscular dystrophy. *Neuromuscul Disord.* 1998;8(2):72-76.
11. Manilal S, Recan D, Sewry CA, et al. Mutations in Emery-Dreifuss muscular dystrophy and their effects on emerin protein expression. *Hum Mol Genet.* 1998;7(5):855-864.
12. Sakata K, Shimizu M, Ino H, et al. High incidence of sudden cardiac death with conduction disturbances and atrial cardiomyopathy caused by a nonsense mutation in the *STA* gene [published online ahead of print June 20, 2005]. *Circulation.* 2005;111(25):3352-3358. doi:10.1161/CIRCULATIONAHA.104.527184.

Human Molecular Genetics, 2007, Vol. 16, No. 15 1884–1895
doi:10.1093/hmg/ddm137
Advance Access published on June 13, 2007

Activation of MAPK in hearts of *EMD* null mice: similarities between mouse models of X-linked and autosomal dominant Emery–Dreifuss muscular dystrophy

Antoine Muchir[1,2], Paul Pavlidis[3,†], Gisèle Bonne[4,5,6], Yukiko K. Hayashi[7] and Howard J. Worman[1,2,*]

[1]Department of Medicine and [2]Department of Anatomy and Cell Biology and [3]Department of Biomedical Informatics, College of Physicians and Surgeons, Columbia University, New York, USA and [4]Institut National de la Santé et de la Recherche Médicale, U582, Institut de Myologie, Paris, France and [5]Université Pierre et Marie Curie-Paris 6, Faculté de médecine, Paris, France and [6]AP-HP, Groupe hospitalier Pitié-Salpêtrière, U.F. Myogénétique et Cardiogénétique, service de Biochimie Métabolique, Paris, France and [7]Department of Neuromuscular Research, National Institute of Neuroscience, National Center of Neurology and Psychiatry, Tokyo, Japan

Received April 25, 2007; Revised and Accepted May 18, 2007

Emery–Dreifuss muscular dystrophy (EDMD) is an inherited disorder characterized by slowly progressive skeletal muscle weakness in a humero-peroneal distribution, early contractures and prominent cardiomyopathy with conduction block. Mutations in *EMD*, encoding emerin, and *LMNA*, encoding A-type lamins, respectively, cause X-linked and autosomal dominant EDMD. Emerin and A-type lamins are proteins of the inner membrane of the nuclear envelope. Whereas the genetic cause of EDMD has been described and the proteins well characterized, little is known on how abnormalities in nuclear envelope proteins cause striated muscle disease. In this study, we analyzed genome-wide expression profiles in hearts from *Emd* knockout mice, a model of X-linked EDMD, using Affymetrix GeneChips. This analysis showed a molecular signature similar to that we previously described in hearts from *Lmna* H222P knock-in mice, a model of autosomal dominant EDMD. There was a common activation of the ERK1/2 branch of the mitogen-activated protein kinase (MAPK) pathway in both murine models, as well as activation of downstream targets implicated in the pathogenesis of cardiomyopathy. Activation of MAPK signaling appears to be a cornerstone in the development of heart disease in both X-linked and autosomal dominant EDMD.

INTRODUCTION

Emery Dreifuss muscular dystrophy (EDMD) is an inherited disorder characterized by contractures of the elbows, Achilles' tendons and spine, slowly progressive wasting and weakness of skeletal muscles in a humero-peroneal distribution (1). Individuals with EDMD also suffer from cardiomyopathy with conduction defects that increases the risk of sudden death. Initially described as an X-linked inherited disorder, autosomal dominant and recessive forms of EDMD are also recognized, with the dominant form being most prevalent.

X-linked EDMD arises as a consequence of mutations in *EMD* on chromosome Xq28 (2). *EMD* encodes emerin, a ubiquitously expressed integral protein of the inner nuclear membrane (3,4). Emerin is composed of 254 amino acids in humans and has a 220 amino acid nucleoplasmic amino-terminal domain, a single transmembrane segment and a short luminal tail (5). Emerin binds to several nuclear proteins

*To whom correspondence should be addressed at: Department of Medicine, College of Physicians and Surgeons, Columbia University, 630 West 168th Street, 10 Floor, Room 508, New York, NY 10032, USA. Tel: +1 2123058156; Fax: +1 2123056443; Email: hjw14@columbia.edu.
†Present address: UBC Bioinformatics Centre, University of British Columbia, Vancouver, Canada BC V6T 1Z4.

and these interactions may underlie various functions attributed to emerin, including regulation of gene expression, nuclear assembly during mitosis, cell cycle control and providing structural support to the nuclear envelope (6). More recently, emerin has also been shown to bind β-catenin and restrict its accumulation in the nucleus (7).

Autosomal EDMD arises from mutations in *LMNA* (8). *LMNA* encodes A-type nuclear lamins, of which lamin A and lamin C are the predominant somatic cell isoforms (9). Nuclear lamins are intermediate filament proteins that polymerize to form a meshwork of 10 nm diameter filaments on the inner aspect of the inner nuclear membrane called the nuclear lamina (10–13). Lamins function in maintaining nuclear architecture and organizing chromatin (14–17). Lamins may also have complex roles in linking the nucleus to the cytoskeleton (18) and in DNA synthesis and transcription regulation (19–21). Lamins interact with integral proteins in the inner nuclear membrane, including emerin, and provide anchorage sites for chromatin and structural support to the nuclear envelope (6,22–27).

Genetically engineered mouse models have been created to study the role of emerin and A-type lamins in the development of EDMD. *Lmna* knockout mice provided the first animal model of the disease (27). The null mice develop cardiomyopathy and regional skeletal muscle wasting reminiscent of human EDMD (27). Subsequently, knock-in mice that express A-type lamins with the H222P (28) and N195K (29) amino acid substitutions were created. Similar to *Lmna* knockout mice, homozygous knock-in animals develop features of human EDMD, including cardiomyopathy; however, heterozygous mice are apparently normal. In transgenic mice, cardiac overexpression of human lamin A M371K leads to heart damage, whereas similar overexpression of wild type human lamin A does not cause significant abnormalities (30). Melcon *et al.* (31) have generated *Emd* null mice, reporting that $Emd^{-/y}$ males are normal at birth and that their subsequent postnatal growth and locomotion are indistinguishable from wild type siblings. These investigators did not report cardiac pathology in $Emd^{-/y}$ mice. Hayashi and colleagues (32) also generated and characterized *Emd* knockout mice and reported that they have a normal growth rate and life span without marked muscle weakness or joint abnormalities but have subtle motor coordination abnormalities. These investigators demonstrated small vacuoles in cardiomyocytes of emerin-deficient mice and detected a slight prolongation of atrioventricular conduction time in $Emd^{-/y}$ mice greater than 40 weeks of age.

Despite the fact that the human genetics have been well described and that relevant animal models have been generated, little is known about how mutations in the genes encoding emerin and A-type lamins lead to striated muscle abnormalities. One strategy that could allow for the identification of molecular abnormalities underlying muscle pathology in animal models of EDMD is comprehensive expression analysis at the transcriptome level using microarrays. Using such methods, Melcon *et al.* (31) have shown that regenerating skeletal muscle from emerin-deficient mice have abnormalities in cell cycle parameters and delayed myogenic differentiation, which is associated with perturbations to transcriptional pathways regulated by the retinoblastoma and MyoD genes. Hence, abnormalities in satellite cell proliferation or differentiation may be responsible for aspects of the pathophysiology of skeletal muscle disease in EDMD by impairing the replacement of fibers. However, this molecular mechanism cannot readily explain cardiac muscle abnormalities, as replacement of cardiomyocytes and regeneration of cardiac tissue is not significant. We recently identified activation of mitogen-activated protein kinase (MAPK) signaling pathway in hearts from mice with the *Lmna* H222P mutation (33). This molecular pathway has been previously implicated in the development of cardiomyopathy and conduction defects (34,35). We now report the results of a genome-wide expression analysis in hearts from *Emd* knockout mice, in which we have identified common molecular alterations found in *Lmna* H222P knock-in mouse hearts, including activation of a MAPK pathway.

RESULTS

Gene expression profiling analysis in hearts from Emd knockout mice

We performed a comparative genome-wide RNA expression analysis in hearts from $Emd^{-/y}$ mice. These mice have mild motor dysfunction, slight prolongation of atrioventricular conduction time and structural fragility of myonuclei (32). We studied mice at 10 weeks of age, before any signs of cardiac dysfunction, to focus on genes with expressions primarily altered as a result of emerin-deficiency and not secondary to possible cardiac damage. At 10 weeks of age, histological analysis of cardiac muscle from $Emd^{-/y}$ mice does not reveal notable pathological changes compared to hearts from control mice (data not shown).

To analyze transcriptomes, we used Affymetrix Mouse Genome 430 2.0 Arrays, which contain 45 101 probes sets for known and predicted genes. We first examined similarities in transcription profiles between hearts from control ($n = 8$) and $Emd^{-/y}$ ($n = 6$) mice by hierarchical cluster analysis. The individual patterns of mRNA signal intensities fell into two distinct groups on a heat map corresponding to the sample genotype, wild type and $Emd^{-/y}$, with similarity between members within each group higher than between the groups (Fig. 1A). This demonstrated that the differences in the distribution of mRNA expression intensities between heart tissue samples from wild type controls and $Emd^{-/y}$ mice were due to changes in the individual gene expression between groups rather than non-specific variations between samples. We then used a supervised learning method to distinguish probe sets representing genes with significant differences in expression between hearts from control and $Emd^{-/y}$ mice. Genes were selected using sufficiently high absolute changes measured by a corrected *t*-test ($q < 0.05$) combined with a one $\log_2$-fold change cut-off. This analysis identified 27 probe sets in hearts from $Emd^{-/y}$ mice, which correspond to 18 upregulated genes and 9 down-regulated genes (Fig. 1B).

The 27 genes with significant differences in expression in hearts of $Emd^{-/y}$ mice compared to control mice are listed in Table 1. Expression of *Emd* encoding emerin was significantly downregulated (1.8 $\log_2$-fold). Several muscle-specific genes were abnormally expressed in hearts from $Emd^{-/y}$ mice.

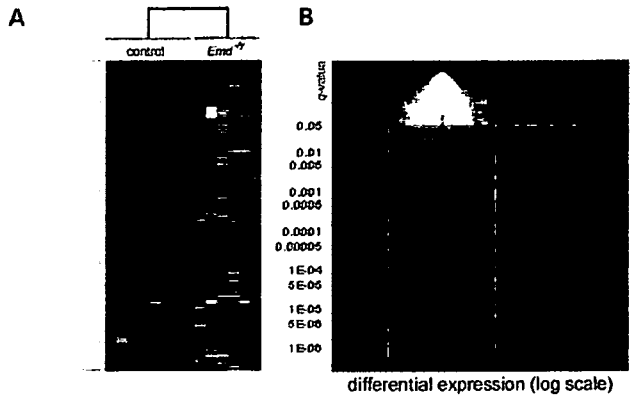

Figure 1. Affymetrix GeneChip expression profiling in hearts of $Emd^{-/y}$ mice. (**A**) Hierarchical clustering analysis of differentially expressed genes in hearts from control and $Emd^{-/y}$ mice. Rows indicate the expression of individual genes and vertical lines indicate each sample. For each gene, the ratio of transcript abundance in the samples to its abundance in the control is represented by color intensities (yellow indicates higher expression and blue indicates lower expression). (**B**) Volcano plots of absolute expression values ($\log_2$[q-value]) determined by robust multichip analysis. For each probe set, expression in hearts from $Emd^{-/y}$ mice is plotted. A two-fold threshold and $q < 0.05$ was used to determine the genes significantly altered in the analysis (yellow line squares).

Genes encoding myosin light chains (*Myl7*, 3.3 $\log_2$-fold; *Myl4*, 2.6 $\log_2$-fold) and myosin heavy chains (*Myh7*, 2.2 $\log_2$-fold) were upregulated. Similarly, there was upregulation of expression of genes encoding sarcolipin (*Sln*, 2.5 $\log_2$-fold), calcium channel L-type (*Cacna1C*, 1.2 $\log_2$-fold) and phospholamban (*Pln*, 1.1 $\log_2$-fold), proteins involved in cardiac contractility. The top-ranked genes identified in this analysis (*Myl4*, *Myl7*, *Myh7*, *Sln*) are common with those previously identified in hearts from $Lmna^{H222P/H222P}$ and $Lmna^{H222P/+}$ mice of the same age (33). Hence, upregulation of several identical gene signatures appears in hearts from animal models of both X-linked and autosomal dominant EDMD before any overt clinical or cardiac pathology.

To independently validate the expression of selected transcripts identified in the microarray analysis, we performed real-time quantitative RT–PCR using RNA extracted from hearts of mice different from those used for the microarrays. Primers corresponding to genes encoding myosin proteins (*Myl4*, *Myl7*, *Myh7*), polyadenylate binding protein-interacting protein 1 (*Paip1*), sarcolipin (*Sln*), peptidylglycine alpha-amidating monooxygenase (*Pam*), transferrin receptor (*Trfc*) and emerin (*Emd*) were selected as representative. Primers for *Emd* were chosen in the 3′ region following the portion of the gene containing the inserted neo^r cassette. For these genes, there was a strong correlation between real-time quantitative RT PCR results and altered expression detected in the microarray analysis of hearts from $Emd^{-/y}$ mice (Fig. 2).

Functional class scoring analysis and ranked gene ontology classes

To obtain a global picture of the affected processes in hearts of $Emd^{-/y}$ mice, we used gene-class testing based on gene ontology (GO) terms. GO terms are functional categories that give information on the known biological processes associated with each gene. Because gene expression might be altered in related groups defined by pathways or functions rather than individually, genes showing coordinated but weak changes may be missed. We therefore used a semi-supervised method called functional class scoring, which examines the statistical distribution of individual gene expression scores among all genes in an ontology class. We can then identify GO terms with significant expression changes for which individual genes involved may not be identified as significant in single gene-profile analysis. Our functional class scoring analysis uses as input the 45 101 q-values from all the probes sets from the Affymetrix Mouse Genome 430 2.0 Arrays without an initial gene selection step. We used two different software packages, ermineJ and Ingenuity Pathway Analysis, which use different statistical approaches (see Materials and Methods).

Using ermineJ, we identified differential expression of GO classes involved in muscle contraction, transcription and translation, metabolism and angiogenesis in hearts from $Emd^{-/y}$ mice (Table 2). GO classes corresponding to signaling pathways were also affected in hearts of $Emd^{-/y}$ mice. These signaling pathways included JNK, MAPK, Wnt, I-kappaB kinase/NF-kappaB and TGF-β (Table 2). Most of the GO classes with altered expression in hearts of $Emd^{-/y}$ mice were previously identified in hearts of $Lmna^{H222P/H222P}$ (33). This suggested common molecular alterations downstream of *Lmna* and *Emd* mutations. Using Ingenuity Pathways Analysis, we identified the same pathways as with ermineJ in the $Emd^{-/y}$ mice. When Ingenuity Pathways Analysis was similarly used to analyze gene expression data from hearts of $Lmna^{H222P/H222P}$ mice (33), it identified genes of several similar pathways affected in hearts of $Emd^{-/y}$ mice (Fig. 3).

MAPK is activated in hearts of Emd knockout mice

Our analysis of functional classes of genes revealed significant differences in expression of the groups of genes encoding proteins of the MAPK pathway in hearts of $Emd^{-/y}$ mice. Because we previously identified activation of MAPK cascade in the *Lmna* H222P knock-in mouse model of autosomal dominant EDMD, we determined if it was similarly activated in hearts of the $Emd^{-/y}$ mouse model of X-linked EDMD. We evaluated the activation of two MAPKs, ERK1/2 and JNK, in hearts from control and $Emd^{-/y}$ mice. These kinases are activated by phosphorylation. Immunoblotting with antibody that recognized phosphorylated ERK1/2 demonstrated an increase in activated ERK1/2 in hearts from $Emd^{-/y}$ mice (Fig. 4A). However, using an antibody that recognized phosphorylated JNK, we did not detect an increase in activated JNK in hearts from $Emd^{-/y}$ mice (Fig. 4A). Phosphorylated ERK1/2 activates a series of downstream target genes, including those encoding elk-1 and atf-2. Immunoblotting with antibodies against elk-1 and atf-2 demonstrated increased expression of atf-2 but not elk-1 in hearts from $Emd^{-/y}$ mice compared to control mice (Fig. 4B). These data indicate an activation of ERK1/2 signaling in hearts from $Emd^{-/y}$ mice.

To compare the degree of ERK1/2 activation in hearts from $Emd^{-/y}$ and $Lmna^{H222P/H222P}$ mice, we measured the activated phosphorylated ERK1/2 by immunoblot. Phosphorylated

Table 1. Genes with altered expression as defined by $q < 0.05$ and ≥ 1 or < -1 $\log_2$-fold change in hearts from *Emd* $^{-/y}$ mice

Probe set name	Gene symbol	Gene name	$\log_2$-fold	q-value
1449071_at	*Myl7*	Myosin, light polypeptide 7, regulatory	3.31	0.0020
1422580_at	*Myl4*	Myosin, light polypeptide 4, alkali; atrial, embryonic	2.55	0.0023
1420884_at	*Sln*	Sarcolipin	2.53	0.0128
1448553_at	*Myh7*	Myosin, heavy polypeptide 7, cardiac muscle, beta	2.12	2.15E-05
1425521_at	*Paip1*	Polyadenylate binding protein-interacting protein 1	1.94	1.62E-05
1454373_x_at	*Ubc*	Ubiquitin C	1.36	0.0132
1418908_at	*Pam*	Peptidylglycine alpha-amidating monooxygenase	1.31	0.0003
1435872_at	*Pim1*	Proviral integration site 1	1.23	0.0069
1420037_at	*Atp5a1*	ATP synthase, H+ transporting, mitochondrial F1 complex, alpha subunit, isoform 1	1.19	0.0294
1452661_at	*Tfrc*	Transferrin receptor	1.19	8.73E-07
1441679_at	*Cacna1c*	Calcium channel, voltage-dependent, L type, alpha 1C subunit	1.17	0.0136
1459238_at	*Pln*	Phospholamban	1.13	0.0163
1449824_at	*Prg4*	Proteoglycan 4 (megakaryocyte stimulating factor, articular superficial zone protein)	1.11	4.03E-06
1421534_at	*Fin15*	Fibroblast growth factor inducible 15	1.10	0.0189
1438714_at	*Zfp207*	Zinc finger protein 207	1.06	0.0146
1425099_a_at	*Arntl*	Aryl hydrocarbon receptor nuclear translocator-like	1.05	3.96E-06
1435602_at	*Sephs2*	Selenophosphate synthetase 2	1.05	0.0186
1432198_at	*6330414g02rik*	RIKEN cDNA 6330414G02 gene	1.02	0.0064
1456746_a_at	*Mic2l1*	MIC2 (monoclonal Imperial Cancer Research Fund 2)-like 1	−1.04	0.0009
1460434_at	*4833415n24rik*	RIKEN cDNA 4833415N24 gene	−1.06	1.14E-05
1416770_at	*Stk25*	Serine/threonine kinase 25 (yeast)	−1.08	0.0009
1449018_at	*Pfn1*	Profilin 1	−1.12	0.0056
1438009_at	*Hist1h2ae*	Histone 1, H2ae	−1.14	8.89E-05
1415997_at	*Txnip*	Thioredoxin interacting protein	−1.36	0.0064
1418174_at	*Dbp*	D site albumin promoter binding protein	−1.39	0.0002
1449526_a_at	*1110015e22rik*	RIKEN cDNA 1110015E22 gene	−1.80	0.0033
1417357_at	*Emd*	Emerin	−1.81	5.40E-08

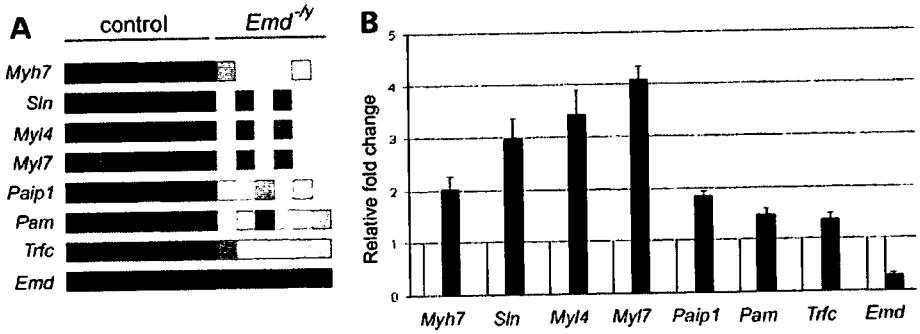

Figure 2. Validation of differential expression in hearts of *Emd* $^{-/y}$ mice of selected genes identified by GeneChips using real-time quantitative RT- PCR. (A) Matrices visualizing Affymetrix GeneChip data of corresponding probe sets of RNAs are shown at left of bar graph. In these matrices, each probe set is visualized as a row of colored squares with one square for each sample. (B) Bars indicate the fold overexpression of the indicated mRNA in hearts measured by real time quantitative RT- PCR as calculated by the $\Delta\Delta C_T$ method. White bars are values corresponding to the control mice and black bars are values corresponding to the *Emd*$^{-/y}$ mice. Values are means ± standard deviations for $n = 4$ samples per group. The real-time quantitative RT- PCR was performed in triplicate with the different RNA samples.

ERK1/2 was activated 2-fold in hearts from *Emd* $^{-/y}$ mice and 3-fold in hearts from *Lmna*$^{H222P/H222P}$ mice compared to hearts from control mice (Fig. 5). This showed a greater activation of ERK1/2 in hearts from *Lmna*$^{H222P/H222P}$ mice than in hearts from *Emd* $^{-/y}$ mice.

We analyzed the expression of additional genes normally activated downstream in the MAPK cascade using real-time quantitative RT-PCR. While these individual genes were not found to be significantly differentially expressed in our single gene-profile analysis, the fact that they are in MAPK GO classes suggested they may be activated. Expression of *c-jun* was statistically significantly increased in hearts from *Emd* $^{-/y}$ mice but expression of *Elk1* and *Elk4* was not (Fig. 6A). We further detected increases in expression of *Atf2*, *Atf4*, *Nfat2* and *Nfat4* in hearts from *Emd* $^{-/y}$ mice (Fig. 6A). To compare this model of X-linked EDMD to a model of autosomal dominant EDMD, we examined the expression of these same genes in hearts from *Lmna*$^{H222P/H222P}$ mice at 10 weeks of age. In hearts from these mice, there was significantly increased expression of all of these downstream factors

Table 2. Top-scoring GO terms listed with corresponding *P*-value and GO identification numbers in hearts from *Emd* $^{-/y}$ mice. The corresponding significant GO classes from *Lmna*$^{H222P/H222P}$ mice are reported

GO term	GO id	*P*-value	
		Emd$^{-/y}$	*Lmna*$^{H222P/H222P}$
Metabolism			
Coenzyme biosynthesis	GO:0009108	9.45E-11	3.97E-03
Phospholipid metabolism	GO:0006644	3.07E-10	7.68E-11
Sulfur metabolism	GO:0006790	1.23E-09	0.0342
Ribonucleotide metabolism	GO:0009259	5.34E-03	0.0204
C21-steroid hormone metabolism	GO:0006700	5.80E-03	0.0204
Organic acid biosynthesis	GO:0016053	6.83E-03	6.73E-03
Vitamin metabolism	GO:0006766	9.10E-03	0.0411
Tricarboxylic acid cycle	GO:0006099	9.83E-03	
Purine nucleotide metabolism	GO:0006163	0.0109	
Fatty acid biosynthesis	GO:0006633	0.0127	1.12E-10
Steroid biosynthesis	GO:0006694	0.0148	4.31E-03
Glycerophospholipid metabolism	GO:0006650	0.0211	
Gluconeogenesis	GO:0006094	0.0215	
Sphingolipid metabolism	GO:0006665	0.0249	4.55E-03
Sterol metabolism	GO:0016125	0.0294	0.0421
Pyruvate metabolism	GO:0006090	0.0310	
Cholesterol metabolism	GO:0008203	0.0316	0.0275
Nucleoside metabolism	GO:0009116	0.0362	
ATP metabolism	GO:0046034	0.0422	
Signaling pathways			
JNK cascade	GO:0007254	1.76E-10	5.12E-11
Rho protein signal transduction	GO:0007266	9.10E-03	
Wnt receptor signaling pathway	GO:0016055	9.22E-03	3.51E-11
Integrin-mediated signaling pathway	GO:0007229	0.0102	
Rac protein signal transduction	GO:0016601	0.0105	0.0116
Transmembrane receptor protein serine/threonine kinase signaling pathway	GO:0007178	0.0222	6.83E-11
I-kappaB kinase/NF-kappaB cascade	GO:0007249	0.0225	5.34E-03
Positive regulation of I-kappaB kinase/NF-kappaB cascade	GO:0043123	0.0310	9.06E-03
Positive regulation of JNK activity	GO:0043507	0.0319	4.39E-03
Activation of MAPK activity	GO:0000187	0.0354	6.30E-03
Transforming growth factor beta receptor signaling pathway	GO:0007179	0.0361	1.76E-10
Frizzled signaling pathway	GO:0007222	0.0483	0.0330
Transcription/translation			
Regulation of translation	GO:0006445	1.54E-10	
Chromatin remodeling	GO:0006338	0.0112	
DNA-dependent DNA replication	GO:0006261	0.0115	0.0111
Positive regulation of transcription, DNA-dependent	GO:0045893	0.0132	2.86E-11
MRNA polyadenylation	GO:0006378	0.0147	0.0271
Regulation of translational initiation	GO:0006446	0.0246	5.27E-03
MRNA 3′-end processing	GO:0031124	0.0262	
DNA methylation	GO:0006306	0.0287	
Muscle contraction			
Striated muscle contraction	GO:0006941	0.0134	3.07E-10
Angiogenesis			
Blood vessel development	GO:0001568	0.0120	2.46E-10
Angiogenesis	GO:0001525	0.0137	2.93E-11
Regulation of angiogenesis	GO:0045765	0.0320	0.0399

in the MAPK cascade (Fig. 6B). These results showed an activation of MAPK pathway in mouse models of X-linked and autosomal dominant EDMD; however, more downstream genes in MAPK pathway were activated in hearts from *Lmna*$^{H222P/H222P}$ mice.

To analyze *in vivo* activation of ERK1/2 in cardiac cells, we used an antibody that recognized phosphorylated ERK1/2 in sections of heart tissue. Histological examination of hearts revealed neither fibrosis nor inflammation or a significant number of cells other than cardiomyocytes (data not shown). Immunofluorescence microscopic labeling of heart sections from control mice with these antibodies revealed a rather diffuse fluorescence pattern, whereas fluorescence in hearts from *Emd* $^{-/y}$ mice was more intense and predominantly nuclear (Fig. 7A). Quantitative analysis of individual cardiomyocytes in the sections confirmed that the anti-phosphorylated ERK antibody labeled both cytoplasm and nucleus in hearts from control mice but essentially only the nucleus in hearts from *Emd*$^{-/y}$ mice (Fig. 7B). While fluorescence intensity of nuclear labeling was significantly higher in cardiomyocytes from *Emd* $^{-/y}$ mice compared to control mice, it was less than that in cardiomyocytes of

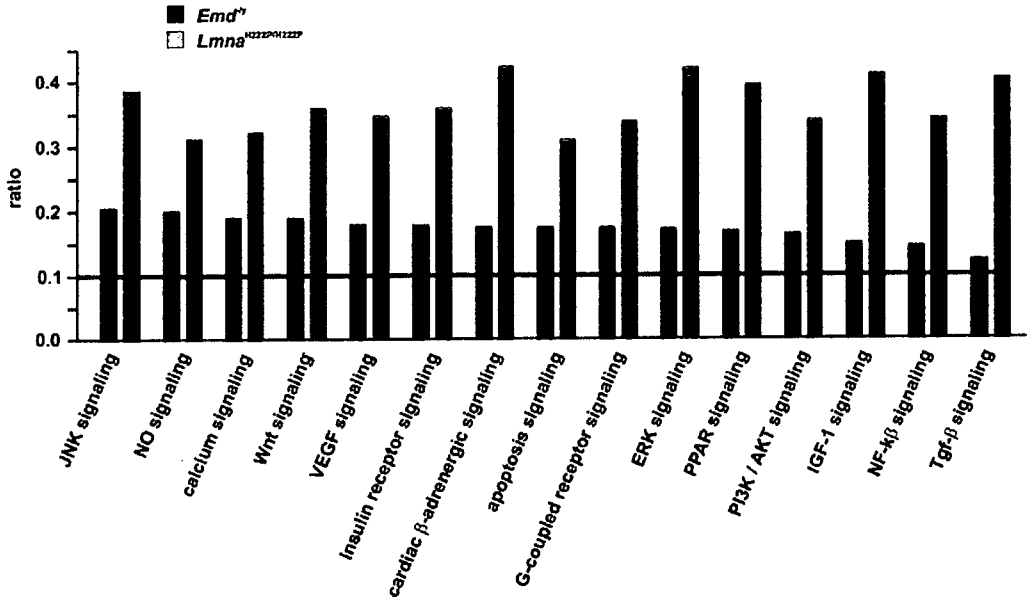

Figure 3. GO analysis of functional groups of genes differentially expressed in hearts of *Emd* $^{-/y}$ and *Lmna*$^{H222P/H222P}$ mice. The most significantly changed GO terms/pathways were identified by canonical pathways analysis using the Ingenuity Pathways Knowledge base. The ratio represents the number of genes from the data set that map to the pathway divided by the number of all known genes ascribed to the pathway.

Lmna$^{H222P/H222P}$ mice (Fig. 7C). These results suggested a gradient of activation and nuclear translocation of ERK1/2 in hearts from *Emd* $^{-/y}$ and *Lmna*$^{H222P/H222P}$ mice compared to control mice.

DISCUSSION

Although the causative genetic mutations have been identified and the descriptive pathology well documented, cellular mechanisms linking the genetic mutations to cardiac dysfunction in EDMD are unknown. We recently showed that in the *Lmna* H222P knock-in mouse model of autosomal dominant EDMD, there was activation of MAPK cascade and downstream targets in heart prior to the development of clinical or histological pathology (33). Genes encoding myosins and other sarcomeric proteins were also abnormally activated in these mice at an age when their hearts were histologically normal (33). In addition to being present in *Lmna*$^{H222P/H222P}$, which develop cardiomyopathy at approximately 8 weeks of age and have shortened life spans, similar early changes in gene expression were present in *Lmna*$^{H222P/+}$ mice, which do not develop significant cardiomyopathy and have normal life spans. In this study, we examined gene expression changes in the hearts of *Emd* $^{-/y}$ mice, a genetic model of X-linked EDMD. Similar to *Lmna*$^{H222P/+}$ mice, these mice apparently have normal life spans and do not develop clinically significant cardiomyopathy; however, they have small vacuoles mostly bordering nuclei in cardiomyocytes and develop mild first-degree heart block at 40 weeks of age (32). The *Emd* $^{-/y}$ mice had gene expression alterations in hearts similar to those in hearts of *Lmna*$^{H222P/+}$ and *Lmna*$^{H222P/H222P}$ mice, including activation of the ERK branch of the MAPK pathway.

It has been hypothesized that dilated cardiomyopathy-causing mutations affect force transmission from the sarcomere to the extra-sarcomeric cytoskeleton (36). In the present study, in which we performed genome-wide expression analysis in hearts from *Emd* $^{-/y}$ mice before any clinical cardiac abnormalities, we showed that genes encoding proteins involved in cardiac contraction are abnormally upregulated. The identified genes encoded either proteins of the sarcomere, such as β-myosin heavy chain and myosin light chain, or proteins involved in the Ca^{2+} homeostasis such as sarcolipin, calcium channel voltage-dependent L type and phospholamban. A concomitant deregulation of these two functional categories acting in muscle excitation-contraction is a common observation in cardiomyopathies (36,37).

We detected an abnormal activation of genes in the MAPK cascade in hearts of *Emd* $^{-/y}$ mice. For some of these genes, we found increased expression only by using real-time RT–PCR. Others and we have previously reported similar differences between microarrays and real-time RT–PCR for transcripts with a low absolute expression or when the difference of expression between the experimental and control are small (33,38,39). The fact that we also showed an increase in phosphorylation and nuclear translocation of ERK1/2 in cardiomyocytes strongly supports an activation of this branch of the MAPK cascade in hearts of *Emd* $^{-/y}$ mice. Although altered expression of the GO group defined as JNK cascade appeared significant in our statistical analysis using eminel and Ingenuity Systems, we did not detect activation of JNK in hearts of *Emd* $^{-/y}$ mice. This could be explained by the redundancy of functional classes in GO analysis. JNK and ERK1/2 are two branches of the MAPK pathway and have been described as activated by similar stimuli through the same G-protein-coupled receptors (40). Both kinases also acti-

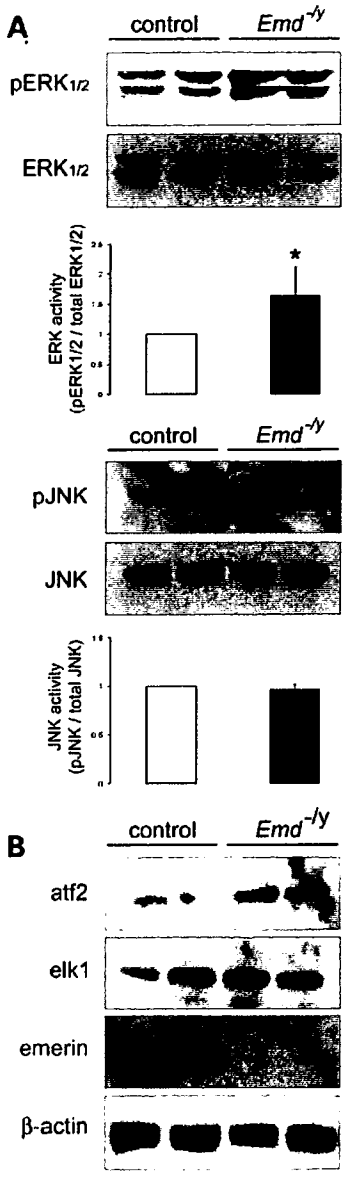

Figure 4. MAPK signaling is activated in hearts from $Emd^{-/y}$ mice. (A) Detection of phosphorylated ERK1/2 (pERK1/2), total ERK1/2, phosphorylated JNK (pJNK) and total ERK1/2 by immunoblotting of proteins extracted from hearts of control and $Emd^{-/y}$ mice. Data in bar graphs are means ± standard deviations for four samples per group (* $P < 0.05$). (B) Detection of elk-1, atf2 and emerin by immunoblotting of proteins extracted from hearts of control and $Emd^{-/y}$ mice. β-actin is used as an internal loading control.

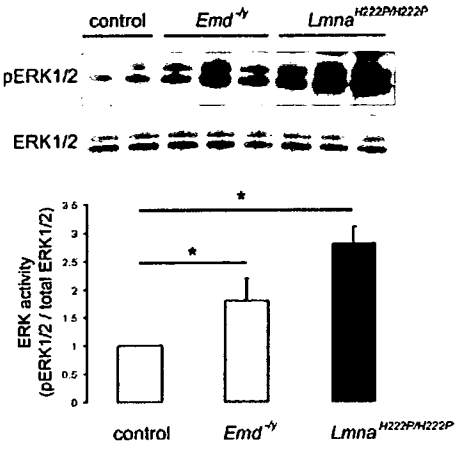

Figure 5. ERK1/2 activation in hearts from both $Emd^{-/y}$ and $Lmna^{H222P/H222P}$ mice. Detection of phosphorylated ERK1/2 (pERK1/2) and total ERK1/2 by immunoblotting of proteins extracted from hearts of control, $Emd^{-/y}$ and $Lmna^{H222P/H222P}$ mice. Data in bar graphs are means ± standard deviations (* $P < 0.05$).

vate the same downstream nuclear substrates (41). The dichotomy between the two branches is not entirely clear and is reflected by 55 probes sets corresponding to 22 genes in both the JNK and ERK1/2 GO functional classes.

Our results further showed that activation of MAPK cascade in hearts of $Emd^{-/y}$ mice was less significant than in hearts of $Lmna^{H222P/H222P}$ mice. We previously demonstrated that both ERK1/2 and JNK were activated in heart from $Lmna^{H222P/H222P}$ mice and to a lesser extent in hearts from $Lmna^{H222P/+}$ mice (33). In this study, we detected only an activation of ERK1/2 in hearts from $Emd^{-/y}$ mouse. We further showed that more downstream targets of MAPK were activated in hearts from $Lmna^{H222P/H222P}$ mice than in hearts from $Emd^{-/y}$ mice. The $Emd^{-/y}$ mice have slight cardiac dysfunction characterized by a mild prolongation of atrioventricular conduction time and vacuolization in cardiomyocytes (32). In contrast, male $Lmna^{H222P/H222P}$ mice develop cardiac chamber dilation associated with decreased left ventricle fractional shortening starting at 8 weeks of age (33). At 12 weeks of age, male $Lmna^{H222P/H222P}$ mice have pronounced conduction system abnormalities characterized by an increased atrioventricular conduction time. Male $Lmna^{H222P/H222P}$ mice die between 4 to 9 months of age. Two hypotheses can be raised to explain these differences between male $Lmna^{H222P/H222P}$ mice and $Emd^{-/y}$ mice. First, activation of the ERK branch of MAPK cascade may ultimately lead only to conduction defects in heart and not to pump failure. This hypothesis remains to be tested. Second, a relationship may exist between the degree of MAPK cascade activation and the severity of the heart disease. Our results suggest that this is more likely to be the case.

Several previous studies have implicated MAPK signaling in the development of cardiomyopathy. Overexpression of members of the ERK branch of MAPK cascade in mice causes cardiomyopathy (41–44). Activation of the MAPK cascade has also been reported in caveolin-3 (45), caveolin-1 (46) and p85 subunit of class I(A) PI3K (47) knockout mice, all of which develop cardiomyopathy. Activating mutations in *MEK1* and *MEK2* encoding kinases that activate ERK1 and ERK2 cause a cardio-facial-cutaneous syndrome (48). In addition, we previously demonstrated that the MAPK cascade is abnormally activated in hearts from *Lmna* H222P knock-in mice (33). The JNK branch of the MAPK cascade is also activated in dilated human hearts (49,50).

The results of this study and our previous work (33) suggest that activation of MAPK results directly from mutations in *Emd* and *Lmna* and that the MAPK activation

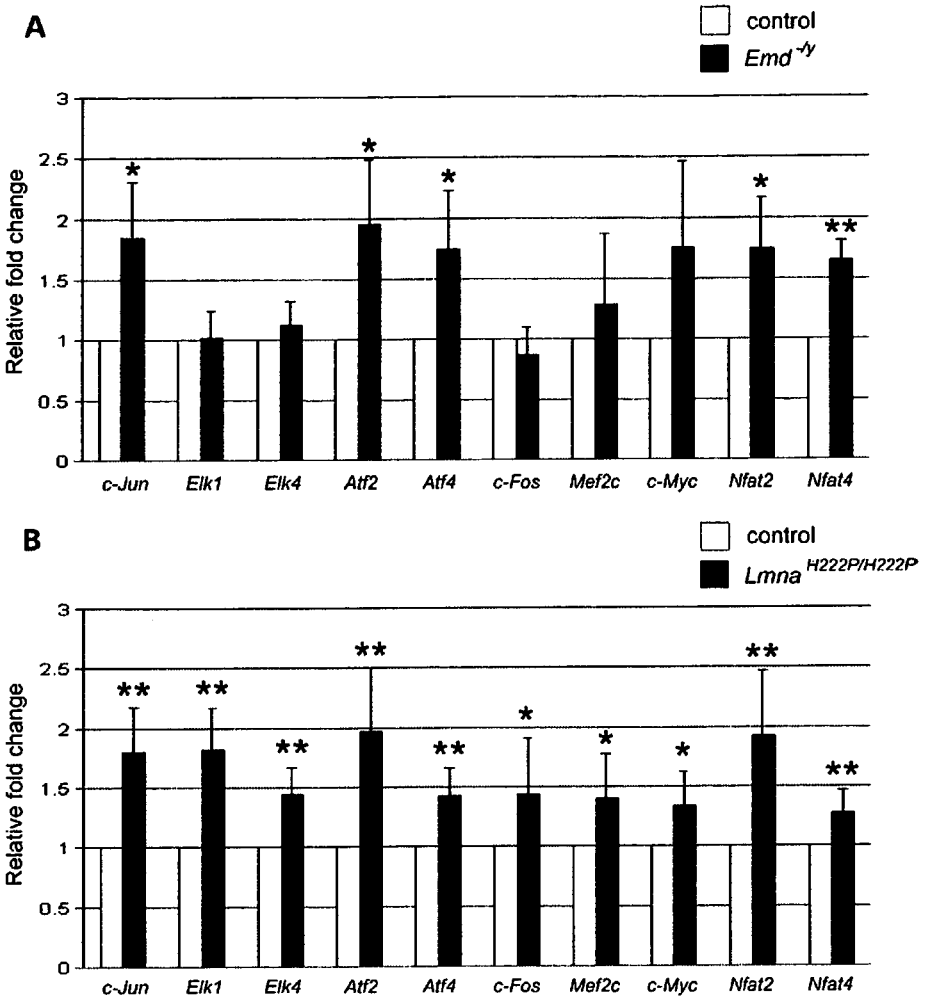

Figure 6. Expression of downstream genes in MAPK pathway in hearts from mouse models of EDMD. (**A**) Summary of real-time RT-PCR results in hearts from *Emd*$^{-/y}$ mice is shown. Bars indicate the fold overexpression of the indicated mRNA normalized to *Gapdh* as calculated by the $\Delta\Delta C_T$ method. Values are means ± standard deviations for $n = 4$ samples per group ($^*P < 0.05$). (**B**) Summary of real-time quantitative RT-PCR results in hearts from *Lmna*$^{H222P/H222P}$ mice is shown. Bars indicate the fold overexpression of the indicated mRNA normalized to *Gapdh* as calculated by the $\Delta\Delta C_T$ method. Values are means ± standard deviations for $n = 4$ samples per group ($^*P < 0.05$, $^{**}P < 0.005$).

leads to heart dysfunction. The mechanism of how mutations in genes encoding nuclear envelope proteins activate MAPK remains to be elucidated; however, ERK and JNK appear to be directly activated by the expression of A-type lamins with amino acid substitutions encoded by *LMNA* mutations that cause autsomal dominant EDMD (33). It remains to be determined if loss of emerin from cells similarly leads directly to MAPK cascade activation. Activation of MAPK leads to the further activation of several downstream target genes and we found several of these, including *c-Jun*, *Atf2*, *Atf4*, *Nfat2* and *Nfat4*, to be abnormally activated in hearts from *Emd* $^{-/y}$ and *Lmna* H222P mice. Transcription factors encoded by these genes can in turn regulate the expression of additional genes, including those encoding proteins involved in sarcomere structure, cardiomyofiber organization and other aspects of heart function (51,52). Abnormal expression of these proteins can lead to cardiomyopathy. Activation of the MAPK cascade has also been previously shown to regulate the calcium induced calcium-released mechanism, producing a negative inotropic effect (53,54). Hence, MAPK activation induced by abnormalities in emerin and A-type lamins can initiate a chain of events that leads to cardiomyopathy.

In summary, our data provide insights into the initial stages of cardiac pathology induced by defects in emerin and A-type lamins. Mutations in the genes encoding these proteins that cause EDMD lead to activation of MAPK signaling in hearts and changes in the expression of downstream genes implicated in the development of cardiomyopathy. These results have important practical implications because small molecule drugs can potentially be used to inhibit the different branches of the MAPK pathway (55,56).

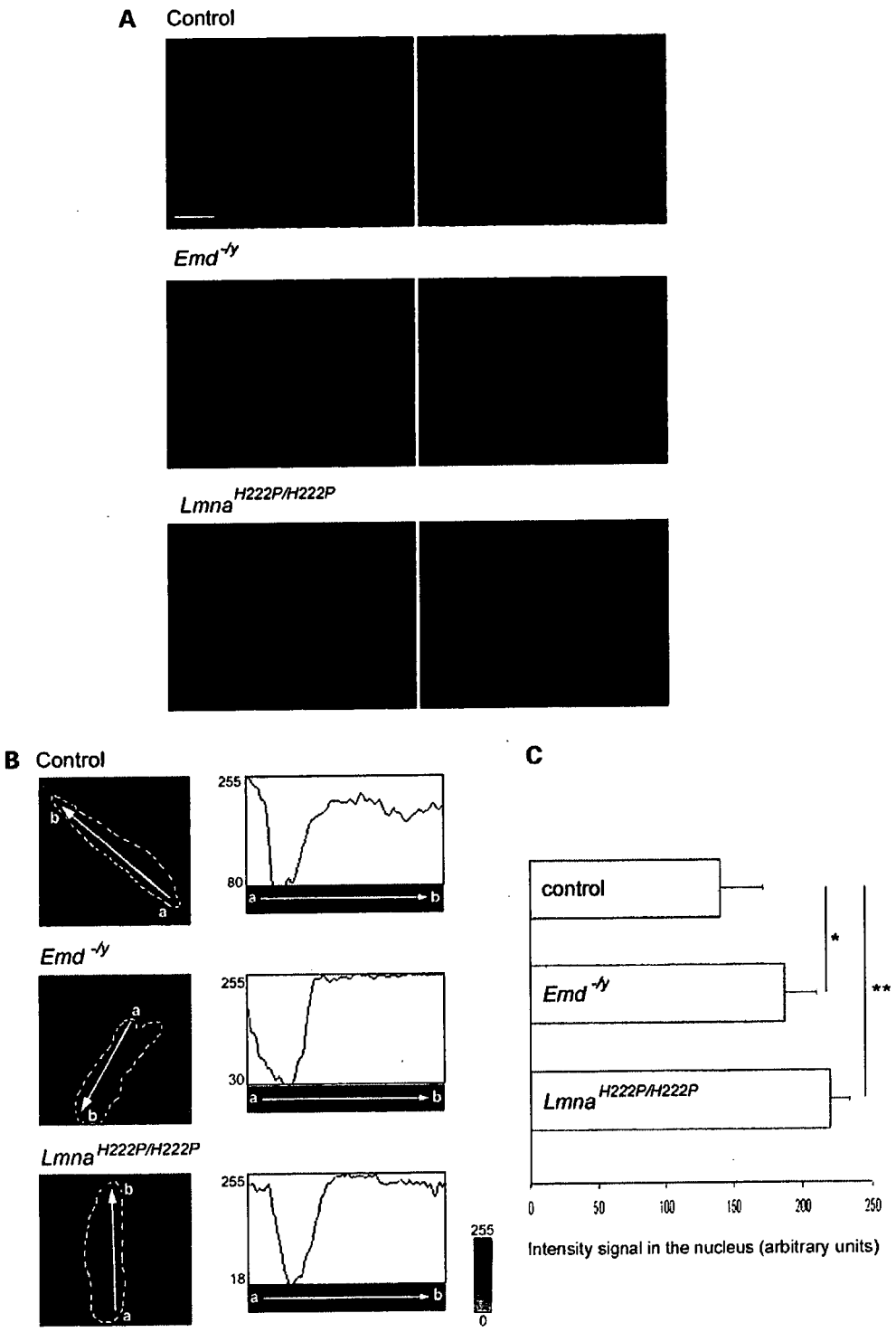

Figure 7. Immunofluorescence microscopic analysis of phopshorylated ERK1/2 (pERK) in heart sections from mouse models of EDMD. (**A**) Sections of frozen heart from control, $Emd^{-/\Delta}$ and $Lmna^{H222P/H222P}$ mice were analyzed by immunofluorescence microscopy using anti-pERK1/2 antibody (red). Sections were counterstained with 4′,6-diamidino-2-phenylindole (blue). Bars: 50 μm. (**B**) Quantification of pERK1/2 labeling in cardiomyocytes from control, $Emd^{-/\Delta}$ and $Lmna^{H222P/H222P}$ mice. Cardiomyocytes are delineated by dotted line and intensity of emitted fluorescence is measured along the yellow arrow (a to b). Intensity of the signal varies from 255 (absence of fluorescence) to 0 as reported on the scale; maximal intensity show on *y*-axis varies between panels. Position of the nucleus and intensity of fluorescence using mouse anti-pERK1/2 antibody is shown in the diagram of a single cardiomyocyte. (**C**) Quantification of pERK1/2 labeling in cardiomyocytes. Bars indicate intensity of pERK1/2 fluorescence in the nucleus of the indicated hearts. Values are means ± standard deviations for the intensity of nuclear fluorescence from $n = 80$ cardiomyocytes from two different hearts per group ($^{*}P < 0.05$, $^{**}P < 0.005$).

MATERIALS AND METHODS

Mice

Emd $^{/y}$ mice (32) and *Lmna*$^{H222P/H222P}$ mice (28) were generated and genotyped as described.

RNA isolation

Total RNA was extracted from mouse hearts using the Rneasy isolation kit (Qiagen) according to the manufacturer's instructions. Adequacy and integrity of extracted RNA were determined by gel electrophoresis and concentrations measured by ultraviolet absorbance spectroscopy.

Microarray processing

We used Mouse Genome 430 2.0 GeneChip Arrays (Affymetrix). cDNA synthesis, cRNA synthesis and labeling were performed as described previously (33). Hybridization, washing, staining and scanning of arrays were performed at the Gene Chip Core Facility of the Columbia University Genome Center.

Microarray data analysis

Image files were obtained through Affymetrix GeneChip software and analyzed by robust multichip analysis using Affymetrix microarray '.cel' image file and GeneTraffic (lobion Informatics) software. Robust multichip analysis is composed of three steps: background correction, quantile normalization and robust probe set summary. Genes were identified as differentially expressed if they met a false discovery rate threshold of 0.05 in a two-sample *t*-test (*q*-value) and showed at least a $\log_2$-fold difference in expression independent of absolute signal intensity. Our gene expression data are available in the National center for Biotechnology Information's Gene Expression Omnibus (GEO; http://www.ncbi.nlm.nih.gov/geo/), accessible through GEO Series accession number GSE6399.

Analysis of functional groups of genes

Gene expression changes related to functional groups were analyzed using the class score method in ermineJ (http://www.bioinformatics.ubc.ca/ermineJ/) (57) and the functional annotation method in Ingenuity Systems software (http://www.ingenuity.com). In ermineJ, the algorithm takes as input the log-transformed *t*-test *P*-values of genes that are members of a single GO class and estimates the probability that the set of *q*-values would occur by chance. Significant GO terms were identified using a false discovery rate of 0.05. In ingenuity systems, the identified canonical pathways were evaluated employing the right-tailed Fisher's exact test to calculate levels of significance. The *P*-value for each pathway was calculated by comparing the number of user-specified genes of interest that participated in a given function or pathway, relative to the total number of occurrences of these genes in all functional/pathway annotations stored in the ingenuity pathways knowledge base. Only annotations that have more Functions/Canonical Pathways Analysis genes than expected by chance ('right-tailed' annotations) were used.

Real-time RT–PCR analysis

Primers were designed correspond to mouse RNA sequences using Primer3 (http://frodo.wi.mit.edu/cgi-bin/primer3/primer3_www.cgi). RNA was extracted using Rneasy Protect Kit (Qiagen) and subsequently reverse transcribed using SuperScript first-strand synthesis system according to the manufacturer's instructions (Invitrogen). The real-time quantitative RT–PCR reaction contained iQ SYBR green super mix (Bio-Rad), 200 nM of primers and 0.2 μl of template in a 25 μl reaction volume. Amplification was carried out using the MyiQ Single-Color real-time PCR Detection System (Bio-Rad) with incubation times of 2 min at 95°C, followed by 50 cycles of 95°C for 30 s and 62°C for 30 s. Specificity of the amplification was checked by melting-curve analysis. Relative levels of mRNA expression were calculated according to the $\Delta\Delta C_T$ method, normalized by comparison to *Gapdh* mRNA expression.

Extraction of proteins from hearts and immunoblotting

Immunoblotting was performed as described previously (33). The following primary antibodies were used at dilutions from 1:200 to 1:1000: mouse monoclonal anti-emerin (Santa-Cruz), rabbit polyclonal anti-ERK1/2 (Santa-Cruz), rabbit polyclonal anti-pERK1/2 (Cell Signaling), rabbit polyclonal anti-JNK (Santa-Cruz), rabbit polyclonal anti-pJNK (Cell Signaling), anti-elk1 (Santa-Cruz), anti-atf-2 (Santa-Cruz) and anti-β-actin (Santa-Cruz). Secondary antibodies were HRP-conjugated (Amersham). Blots were developed using ECL (GE Healthcare) and exposed to X-OMAT film (Kodak) for appropriate periods of time. Band densities were calculated using Scion Image software (Scion Corporation) and normalized to the appropriate total JNK or ERK1/2 of protein extracts.

Immunofluorescence microscopy

For immunohistochemistry, 8 μm frozen sections of transversal cardiac muscles were fixed in 3.7% formaldehyde in phosphate-buffered saline for 15 min and then blocked in 5% fetal goat serum in phosphate-buffered saline containing 0.5% Triton X-100 for 1 h. Antibodies used were primary mouse anti-pERK1/2 (Cell Signaling) and secondary Texas Red conjugated anti-mouse (Molecular Probes). Sections were counterstained with 0.1 μg/ml 4′,6-diamidino-2-phenylindole (Sigma-Aldrich). Specimens were observed using a Microphot SA (Nikon). Images were collected using a Spot RT Slide camera (Diagnostic Instruments) linked to a PC computer running Adobe Photoshop 6.0 (Adobe Systems). Fluorescence intensity in cardiomyocytes was measured using Scion Image software (Scion Corporation). Data are reported as means ± standard deviations and are compared with respective controls using a two-tailed *t*-test.

ACKNOWLEDGEMENTS

We thank T. Arimura and V. Decostre for assistance with breeding and analyzing *Lmna* H222P mice, A. Gharavi for assistance with real-time quantitative RT–PCR, V. Miljkovic for assistance with hybridization of Affymetrix GeneChips

and J. Ribeiro, C. Derognat and S. Mafray for helpful discussions. A.M. was supported in part by fellowship grants from Association Française contre les Myopathies and Fondation pour la Recherche Médicale. This work was supported primarily by a grant from the National Institutes of Health (AR048997) to H.J.W. It was also supported by grants for Research on Psychiatric and Neurological Diseases and Mental Health from Health and Labor Sciences Research, Scientific Research from the Japan Society for the Promotion of Science and the Nervous and Mental Disorders and from the Japan Ministry of Health, Labor and Welfare to Y.K.H.; from the Human Frontiers Science Program (RGP0057/2001-M) to H.J.W., Y.K.H. and G.B.; and from the European Union Sixth Framework (Euro-laminopathies, Contract No. 018690) and from Association Française contre les Myopathies (No. 11057) to G.B.

Conflict of Interest statement. None declared.

REFERENCES

1. Emery, A.E.H. (2000) Emery–Dreifuss muscular dystrophy—a 40 year retrospective. *Neuromusc. Disord.*, **10**, 228–232.
2. Bione, S., Maestrini, E., Rivella, S., Mancini, M., Regis, S., Romeo, G. and Toniolo, D. (1994) Identification of a novel X-linked gene responsible for Emery–Dreifuss muscular dystrophy. *Nat. Genet.*, **8**, 323–327.
3. Nagano, A., Koga, R., Ogawa, M., Kurano, Y., Kawada, J., Okada, R., Hayashi, Y.K., Tsukahara, T. and Arahata, K. (1996) Emerin deficiency at the nuclear membrane in patients with Emery–Dreifuss muscular dystrophy. *Nat. Genet.*, **12**, 254–259.
4. Manilal, S., Nguyen, T.M., Sewry, C.A. and Morris, G.E. (1996) The Emery–Dreifuss muscular dystrophy protein, emerin, is a nuclear membrane. *Hum. Mol. Genet.*, **5**, 801–808.
5. Cartegni, L., Di Barletta, M.R., Barresi, R., Squarzoni, S., Sabatelli, P., Maraldi, N., Mora, M., Di Blasi, C., Comelio, F., Merlini, L. *et al.* (1997) Heart specific localization of emerin: new insights into Emery–Dreifuss muscular dystrophy. *Hum. Mol. Genet.*, **6**, 2257–2264.
6. Bengtsson, L. and Wilson, K.L. (2004) Multiple and surprising new functions for emerin, a nuclear membrane protein. *Curr. Opin. Cell Biol.*, **16**, 73–79.
7. Markiewicz, E., Tilgner, K., Barker, N., van de Wetering, M., Clevers, H., Dorobek, M., Hausmanowa-Petrusewicz, I., Ramaekers, F.C.S., Broers, J.L.V., Blankesteijn, W.M. *et al.* (2006) The inner nuclear membrane protein emerin regulates β-catenin activity by restricting its accumulation in the nucleus. *EMBO J.*, **25**, 3275–3285.
8. Bonne, G., Di Barletta, M.R., Varnous, S., Becane, H.M., Hammouda, E.H., Merlini, L., Muntoni, F., Greenberg, C.R., Gary, F., Urtizberea, J.A. *et al.* (1999) Mutations in the gene encoding lamin A/C cause autosomal dominant Emery–Dreifuss muscular dystrophy. *Nat. Genet.*, **21**, 285–288.
9. Lin, F. and Worman, H.J. (1993) Structural organization of the human gene encoding nuclear lamin A and nuclear lamin C. *J. Biol. Chem.*, **268**, 16321–16326.
10. McKeon, F.D., Kirschner, M.W. and Caput, D. (1986) Homologies in both primary and secondary structure between nuclear envelope and intermediate filament proteins. *Nature*, **319**, 463–468.
11. Fisher, D.Z., Chaudhary, N. and Blobel, G. (1986) cDNA sequencing of nuclear lamins A and C reveals primary and secondary structural homology to intermediate filament proteins. *Proc. Natl Acad. Sci. USA*, **83**, 6450–6454.
12. Aebi, U., Cohn, J., Buhle, L. and Gerace, L. (1986) The nuclear lamina is a meshwork of intermediate-type filaments. *Nature*, **323**, 560–564.
13. Goldman, A.E., Maul, G., Steinert, P.M., Yang, H.Y. and Goldman, R.D. (1986) Keratin-like proteins that co-isolate with intermediate filaments of BHK-21 cells are nuclear lamins. *Proc. Natl Acad. Sci. USA*, **83**, 3839–3843.
14. Liu, J., Rolef Ben-Shahar, T., Riemer, D., Treinin, M., Spann, P., Weber, K., Fire, A. and Gruenbaum, Y. (2000) Essential roles for *Caenorhabditis elegans* lamin gene in nuclear organization, cell cycle progression, and spatial organization of nuclear pore complexes. *Mol. Biol. Cell.*, **11**, 3937–3947.
15. Muchir, A., van Engelen, B.G., Lammens, M., Mislow, J.M., McNally, E., Schwartz, K. and Bonne, G. (2003) Nuclear envelope alterations in fibroblasts from LGMD1B patients carrying nonsense Y259X heterozygous or homozygous mutation in lamin A/C gene. *Exp. Cell Res.*, **291**, 352–362.
16. Muchir, A., Medioni, J., Laluc, M., Massart, C., Arimura, T., van Der Kooi, A.J., Desguerre, I., Mayer, M., Ferrer, X., Briault, S. *et al.* (2004) Nuclear envelope alterations in fibroblasts from patients with muscular dystrophy, cardiomyopathy and partial lipodystrophy carrying lamin A/C gene mutations. *Muscle Nerve*, **30**, 444–450.
17. Vigouroux, C., Auclair, M., Dubosclard, E., Pouchelet, M., Capeau, J., Courvalinn, J.C. and Buendia, B. (2001) Nuclear envelope disorganization in fibroblasts from lipodystrophic patients with heterozygous R482Q/W mutations in lamin A/C gene. *J. Cell Sci.*, **114**, 4459–4468.
18. Worman, H.J. and Gundersen, G.G. (2006) Here come the SUNs: a nucleocytoskeletal missing link. *Trends Cell Biol.*, **16**, 67–69.
19. Spann, T.P., Moir, R.D., Goldman, A.E., Stick, R. and Goldman, R.D. (1997) Disruption of nuclear lamin organization alters the distribution of replication factors and inhibits DNA synthesis. *J. Cell Biol.*, **136**, 1201–1212.
20. Moir, R.D., Spann, T.P., Herrmann, H. and Goldman, R.D. (2000) Disruption of nuclear lamin organization blocks the elongation phase of DNA replication. *J. Cell Biol.*, **149**, 1179–1192.
21. Spann, T.P., Goldman, A.E., Wang, C., Huang, S. and Goldman, R.D. (2002) Alteration of nuclear lamin organization inhibits RNA polymerase II-dependent transcription. *J. Cell Biol.*, **156**, 603–608.
22. Worman, H.J. and Courvalin, J.C. (2000) The inner nuclear membrane. *J. Membr. Biol*, **177**, 1–11.
23. Fairley, E.A., Kendrick-Jones, J. and Ellis, J.A. (1999) The Emery–Dreifuss muscular dystrophy phenotype arises from aberrant targeting and binding of emerin at the inner nuclear membrane. *J. Cell Sci.*, **112**, 2571–2582.
24. Clements, L., Manilal, S., Love, D.R. and Morris, G.E. (2000) Direct interaction between emerin and lamin A. *Biochem. Biophys. Res. Commun.*, **267**, 709–714.
25. Sakaki, M., Koike, H., Takahashi, N., Sasagawa, N., Tomioka, S., Arahata, K. and Ishiura, S. (2001) Interaction between emerin and nuclear lamins. *J. Biochem.*, **129**, 321–327.
26. Muchir, A. and Worman, H.J. (2004) The nuclear envelope and human disease. *Physiology*, **19**, 309–314.
27. Sullivan, T., Escalante-Alcalde, D., Bhatt, H., Anver, M., Bhat, N., Nagashima, K., Stewart, C.L. and Burke, B. (1999) Loss of A-type lamin expression compromises nuclear envelope integrity leading to muscular dystrophy. *J. Cell Biol.*, **147**, 913–920.
28. Arimura, T., Helbling-Leclerc, A., Massart, C., Varnous, S., Niel, F., Lacène, F., Fromes, Y., Toussaint, M., Mura, A-M., Keller, D.I. *et al.* (2005) Mouse model carrying H222P-*Lmna* mutation develops muscular dystrophy and dilated cardiomyopathy similar to human striated muscle laminopathies. *Hum. Mol. Genet.*, **14**, 155–169.
29. Mounkes, L.C., Kozlov, S.V., Rottman, J.N. and Stewart, C.L. (2005) Expression of an *LMNA*-N195K variant of A-type lamins results in cardiac conduction defects and death in mice. *Hum. Mol. Genet.*, **14**, 2167–2180.
30. Wang, Y., Herron, A.J. and Worman, H.J. (2006) Pathology and nuclear abnormalities in hearts of transgenic mice expressing M371K lamin A encoded by an *LMNA* mutation causing Emery–Dreifuss muscular dystrophy. *Hum. Mol. Genet.*, **15**, 2479–2489.
31. Melcon, G., Kozlov, S., Cutler, D.A., Sullivan, T., Hernandez, L., Zhao, P., Mitchell, S., Nader, G., Bakay, M., Rottman, J.N. *et al.* (2006) Loss of emerin at the nuclear envelope disrupts the Rb1/E2F and MyoD pathways during muscle regeneration. *Hum. Mol. Genet.*, **15**, 637–651.
32. Ozawa, R., Hayashi, Y.K., Ogawa, M., Kurokawa, R., Matsumoto, H., Noguchi, S., Nonaka, I. and Nishino, I. (2006) Emerin-lacking mice show minimal motor and cardiac dysfunctions with nuclear-associated vacuoles. *Am. J. Pathol.*, **168**, 907–917.
33. Muchir, A., Pavlidis, P., Decostre, V., Herron, A.J., Arimura, T., Bonne, G. and Worman, H.J. (2007) Activation of MAPK pathway links *LMNA* mutations to cardiomyopathy in Emery–Dreifuss muscular dystrophy. *J. Clin. Invest.*, **117**, 1282–1293.

34. Petrich, B.G., Gong, X., Lerner, D.L., Wang, X., Brown, J.H., Saffitz, J.E. and Wang, Y. (2002) c-Jun N-terminal kinase activation mediates downregulation of connexin43 in cardiomyocytes. *Circ. Res.*, **91**, 640–647.
35. Petrich, B.G., Molkentin, J.D. and Wang, Y. (2003) Temporal activation of c-Jun N-terminal kinase in adult transgenic heart via cre-loxP-mediated DNA recombination. *FASEB J.*, **17**, 749–751.
36. Morita, H., Seidman, J. and Seidman, C.E. (2005) Genetic causes of human heart failure. *J. Clin. Invest.*, **115**, 518–526.
37. Yano, M., Ikeda, Y. and Matsuzaki, M. (2005) Altered intracellular Ca2+ handling in heart failure. *J. Clin. Invest.*, **115**, 556–564.
38. Qin, L.X., Beyer, R.P., Hudson, F.N., Linford, N.J., Morris, D.E. and Kerr, K.F. (2006) Evaluation of methods for oligonucleoyides array data via quantitative real time PCR. *BMC Bioinformatics*, **7**, 23.
39. Millenaar, F.F., Okyere, J., May, S.T., van Zanten, M., Voesenek, L.A. and Peeters, A.J. (2006) How to decide? Different methods of calculating gene expression from short oligonucleotide array data will give different results. *BMC Bioinformatics*, **7**, 137.
40. Michel, M.C., Li, Y. and Heusch, G. (2001) Mitogen-activated protein kinases in the heart. *Naunyn Schmiedebergs Arch. Pharmacol.*, **363**, 245–266.
41. Liang, Q. and Molkentin, J.D. (2003) Redefining the roles of p38 and JNK signaling in cardiac hypertrophy: dichotomy between cultured myocytes and animals models. *J. Mol. Cell. Cardiol*, **35**, 1385–1394.
42. Braz, J.C., Bueno, O.F., Liang, Q., Wilkins, B.J., Dai, Y.S., Parsons, S., Braunwart, J., Glascock, B.J., Klevitsky, R., Kimball, T.F. *et al.* (2003) Targeted inhibition of p38 MAPK promotes hypertrophic cardiomyopathy through upregulation of calcineurin-NFAT signaling. *J. Clin. Invest.*, **111**, 1475–1486.
43. Nicol, R.L., Frey, N., Pearson, G., Cobb, M., Richardson, J. and Olson, E.N. (2001) Activated MEK5 induces serial assembly of sarcomeres and eccentric cardiac hypertrophy. *EMBO J.*, **20**, 2757–2767.
44. Bueno, O.F., De Windt, L.J., Tymitz, K.M., Witt, S.A., Kimball, T.R., Klevitsky, R., Hewett, T.E., Jones, S.P., Lefer, D.J., Peng, C.F. *et al.* (2000) The MEK1-ERK1/2 signaling pathway promotes compensated cardiac hypertrophy in transgenic mice. *EMBO J.*, **19**, 6341–6350.
45. Woodman, S.E., Park, D.S., Cohen, A.W., Cheung, M.W., Chandra, M., Shirani, J., Tang, B., Jelicks, L.A., Kitsis, R.N., Christ, G.J. *et al.* (2002) Caveolin-3 knock-out mice develop a progressive cardiomyopathy and show hyperactivation of the p42/44 MAPK cascade. *J. Biol. Chem.*, **277**, 38988–38997.
46. Cohen, A.W., Park, D.S., Woodman, S.E., Williams, T.M., Chandra, M., Shirani, J., Pereira de Souza, A., Kitsis, R.N., Russell, R.G., Weiss, L.M. *et al.* (2003) Caveolin-1 null mice develop cardiac hypertrophy with hyperactivation of p42/44 MAP kinase in cardiac fibroblasts. *Am. J. Physiol. Cell. Physiol.*, **284**, 457–474.
47. Luo, J., McMullen, J.R., Sobkiw, C.L., Zhang, L., Dorfman, A.L., Sherwood, M.C., Logsdon, M.N., Horner, J.W., DePinho, R.A., Izumo, S. *et al.* (2005) Class IA phosphoinositide 3-kinase regulates heart size and physiological cardiac hypertrophy. *Mol. Cell. Biol.*, **25**, 9491–9502.
48. Rodriguez-Viciana, P., Tetsu, O., Tidyman, W.E., Estep, A.L., Conger, B.A., Santa Cruz, M., McCormick, F. and Rauen, K.A. (2006) Germline mutations in genes within the MAPK pathway cause cardio-facio-cutaneous syndrome. *Science*, **311**, 1287–1290.
49. Cook, S.A., Sugden, P.H. and Clerk, A. (1999) Activation of c-Jun N-terminal kinases and p38-mitogen-activated protein kinases in human heart failure secondary to ischaemic heart disease. *J. Mol. Cell. Cardiol.*, **31**, 1429–1434.
50. Haq, S., Choukroun, G., Lim, H., Tymitz, K.M., del Monte, F., Gwathmey, J., Grazette, L., Michael, A., Hajjar, R., Force, T. *et al.* (2001) Differential activation of signal transduction pathways in human hearts with hypertrophy versus advanced heart failure. *Circulation*, **103**, 670–677.
51. Gillespie-Brown, J., Fuller, S.J., Bogoyevitch, M.A., Cowley, S. and Sugden, P.H. (1995) The mitogen-activated protein kinase kinase MEK1 stimulates a pattern of gene expression typical of the hypertrophic phenotype in rat ventricular cardiomyocytes. *J. Biol. Chem.*, **270**, 28092–28096.
52. Thorburn, J., Carlson, M., Mansour, S.J., Chien, K.R., Ahn, N.G. and Thorburn, A. (1995) Inhibition of a signaling pathway in cardiac muscle cells by active mitogen-activated protein kinase kinase. *Mol. Biol. Cell.*, **6**, 1479–1490.
53. Liao, P., Wang, S.Q., Wang, S., Zheng, M., Zheng, M., Zhang, S.J., Cheng, H., Wang, Y. and Xiao, R.P. (2002) p38 mitogen-activated protein kinase mediates a negative inotropic effect in cardiac myocytes. *Circ. Res.*, **90**, 190–196.
54. Menick, D.R., Xu, L., Kappler, C., Jiang, W., Withers, P., Shepherd, N., Conway, S.J. and Muller, J.G. (2002) Pathways regulating Na+/Ca2+ exchanger expression in the heart. *Ann. N.Y. Acad. Sci.*, **976**, 237–247.
55. English, J.M. and Cobb, M.H. (2002) Pharmacological inhibitors of MAPK pathways. *Trends Pharmacol. Sci*, **23**, 40–45.
56. Bogoyevitch, M.A., Boehm, I., Oakley, A., Ketterman, A.J. and Barr, R.K. (2004) Targeting the JNK MAPK cascade for inhibition: basic science and therapeutic potential. *Biochim. Biophys. Acta*, **1697**, 89–101.
57. Lee, H.K., Braynen, W., Keshav, K., and Pavlidis, P. (2005) ErmineJ: tool for functional analysis of gene expression data sets. *BMC Bioinformatics*, **6**, 269.

FEBS Letters 582 (2008) 1189–1196

Affixin activates Rac1 via βPIX in C2C12 myoblast

Chie Matsuda[a,b,*], Kimihiko Kameyama[a], Atsushi Suzuki[c], Wataru Mishima[d], Satoshi Yamaji[d], Harumasa Okamoto[a], Ichizo Nishino[b], Yukiko K. Hayashi[b]

[a] *Neuroscience Research Institute, AIST, Central 6, 1-1-1 Higashi, Tsukuba, Ibaraki 305-8566, Japan*
[b] *Department of Neuromuscular Research, National Institute of Neuroscience, NCNP, Ogawa-Higashi, Kodaira, Tokyo 187-8502, Japan*
[c] *Department of Molecular Biology, Yokohama City University, Graduate School of Medicine, 3-9 Fukuura, Kanazawa-ku, Yokohama 236-0004, Japan*
[d] *Department of Internal Medicine and Clinical Immunology, Yokohama City University, Graduate School of Medicine, 3-9 Fukuura, Kanazawa-ku, Yokohama 236-0004, Japan*

Received 25 December 2007; accepted 31 January 2008

Available online 4 March 2008

Edited by Berend Wieringa

Abstract Affixin/β-parvin is an integrin-linked kinase (ILK)-binding focal adhesion protein highly expressed in skeletal muscle and heart. To elucidate the possible role of affixin in skeletal muscle, we established stable C2C12 cell line expressing T7-tagged human affixin (C2C12-affixin cells). Exogenous expression of affixin promotes lamellipodium formation where affixin, ILK αp21-activated kinase (PAK)-interactive exchange factor (PIX) and βPIX accumulate. The association of affixin and βPIX was confirmed by immunoprecipitation and pull down assay. In C2C12-affixin cells, an increased level of activated Rac1 but not Cdc42 was observed, and mutant βPIX lacking guanine nucleotide exchange factor activity inhibited lamellipodium formation. These results suggest that affixin is involved in reorganization of subsarcolemmal cytoskeletal actin by activation of Rac1 through α and βPIXs in skeletal muscle.

Structured summary:
MINT-6179203, MINT-6179212, MINT-6178859, MINT-6178812, MINT-6178832, MINT-6178843:
Affixin (uniprotkb:Q9HBI1) *physically interacts* (MI:0218) with *βpix* (uniprotkb:Q9ES28) by *coimmunoprecipitation* (MI:0019)
MINT-6179221:
Affixin (uniprotkb:Q9HBI1) *physically interacts* (MI:0218) with *αpix* (uniprotkb:Q8K4I3) by *coimmunoprecipitation* (MI:0019)
MINT-6178962, MINT-6178983:
Affixin (uniprotkb:Q9HBI1) *physically interacts* (MI:0218) with *βpix* (uniprotkb:Q9ES28) by *pull-down* (MI:0096)
MINT-6179002, MINT-6179021:
Affixin (uniprotkb:Q9HBI1) *binds* (MI:0407) *βpix* (uniprotkb:Q9ES28) by *pull-down* (MI:0096)
MINT-6179039:
PAK1 (uniprotkb:Q13153) *physically interacts* (MI:0218) with *Rac1* (uniprotkb:P63001) by *pull-down* (MI:0096)
MINT-6179054:
PAK1 (uniprotkb:Q13153) *physically interacts* (MI:0218) with *Cdc42* (uniprotkb:P70766) by *pull-down* (MI:0096)
MINT-6178790:
Affixin (uniprotkb:Q9HBI1) and *αpix* (uniprotkb:Q8K4I3) *colocalize* (MI:0403) by *fluorescence microscopy* (MI:0416)
MINT-6178760:
Affixin (uniprotkb:Q9HBI1) and *βpix* (uniprotkb:Q9ES28) *colocalize* (MI:0403) by *fluorescence microscopy* (MI:0416)
MINT-6178801:
Affixin (uniprotkb:Q9HBI1) and *dysferlin* (uniprotkb:Q9ESD7) *colocalize* (MI:0403) by *fluorescence microscopy* (MI:0416)
MINT-6178779:
Affixin (uniprotkb:Q9HBI1) and *ILK* (uniprotkb:O55222) *colocalize* (MI:0403) by *fluorescence microscopy* (MI:0416)

Keywords: Affixin/β-parvin; Lamellipodia; βPIX; Cytoskeletal actin

1. Introduction

Affixin/β-parvin (affixin) [1,2] is one of family of parvin family together with α-parvin/actopaxin/CH-ILKBP [1,3,4], and γ-parvin [1]. Parvins contain two caponin-homology (CH) domains and are known to have important role in focal adhesion, cell spreading and motility [5]. Our previous results revealed that affixin associates with αp21-activated kinase (PAK)-interactive exchange factor (PIX)/ARHGEF6/Cool-2 (αPIX) at the tips of lamellipodia of motile cells and transmits integrin-ILK signals which activate Cdc42 and Rac1, small Rho GTPases [6]. We also showed affixin directly binds to α-actinin which has a crucial role in reorganization of cytoskeletal actin [7]. Affixin is a protein highly expressed in skeletal muscle, and mainly localizes at sarcolemma [2]. We previously reported reduced sarcolemmal staining of affixin in dysferlin deficient skeletal muscles, and confirmed the association between affixin and dysferlin by an immunoprecipitation study [8]. Dysferlin is a sarcolemmal protein and its deficiency causes Miyoshi myopathy and limb girdle muscular dystrophy type 2B [9,10]. Based on the observation of

*Corresponding author. Fax: +81 29 861 6482.
E-mail address: c-matsuda@aist.go.jp (C. Matsuda).

Abbreviations: ILK, integrin-linked kinase; PIX, PAK-interactive exchange factor; C2C12-affixin, stable C2C12 cell line expressing T7-tagged human affixin; GEF, guanine nucleotide exchange factor; GST, gulutathione S-transferase; CH, caponin-homology; DH, Dbl-homology; PH, pleckstrin-homology; PAK, p21-activated kinase; CHO, Chinese hamster ovary

0014-5793/$34.00
doi:10.1016/j.febslet.2008.01.064

dysferlin accumulation at wounded sarcolemmal sites, dysferlin is suggested to have an important role in Ca^{2+}-induced membrane repair [11]. These results imply participation of affixin in membrane repair process of skeletal muscle together with dysferlin, although the precise biological function of affixin in skeletal muscle is not yet clear.

In this study, we established stable C2C12 myoblast cell lines expressing human affixin (C2C12-affixin cells) to elucidate the possible role of affixin in skeletal muscle. The C2C12 myoblast is derived from mouse satellite cell and widely used as an in vitro model for skeletal muscle [12]. Here we show that exogenous overexpression of affixin promotes lamellipodium formation. In the C2C12-affixin cells, affixin is co-localized with βPIX/ARHGEF7/Cool-1 (βPIX) at lamellipodia together with αPIX, ILK and dysferlin. βPIX is a close homolog of αPIX and known to induce membrane ruffling [13]. The interaction of affixin with βPIX is confirmed by immunoprecipitation and pulldown assay. The level of activated Rac1 increased in the C2C12-affixin cells compared to C2C12 cells. Lamellipodium formation of the C2C12-affixin cells is suppressed by transfection of mutant αPIX or βPIX lacking guanine nucleotide exchange factor (GEF) activity. These results suggest an important role of affixin in subsarcolemmal actin reorganization by activation of Rac1 through α and βPIXs in skeletal muscle.

2. Materials and methods

2.1. Cell culture and establishment of stable transfectant

C2C12 myoblasts and COS-7 cells were maintained at 37 °C in a humidified atmosphere of 5% CO_2 in Dulbecco's modified Eagle's medium (Sigma) supplemented with 10% fetal bovine serum. C2C12 cells were transfected with T7-tagged human affixin cDNA subcloned into pcDNA3.1 (Invitrogen) using Lipofectamine 2000 (Invitrogen). All construct sequences were verified with DNA sequencing using ABI PRISM 310 (Applied Biosystems). The cells expressing T7-tagged human affixin were selected in growth media with 1 mg/ml G418 (Invitrogen). The surviving colonies were isolated and separately amplified. Cell line maintenance was performed with 0.5 mg/ml G418.

2.2. Antibodies

Monoclonal antibody against human dysferlin (NCL-Hamlet-2) was purchased from Novocastra. Rabbit polyclonal antibody against human affixin was previously characterized [2]. Rabbit polyclonal antibody against human αPIX was generated as described previously by Manser et al. [13]. We confirmed that affinity-purified anti-αPIX antibody did not cross-react with human βPIX expressed in COS-7 cells. Anti-ILK monoclonal antibody (Upstate Biotechnology), anti-βPIX polyclonal antibody (Chemicon International), anti-βPIX monoclonal antibody (BD Transduction Laboratories), anti-T7 polyclonal antibody (Omni-probe; Santa Cruz), anti-T7 monoclonal antibody (Novagen), anti-HA rat monoclonal antibody (3F10; Roche), anti-HA monoclonal antibody (262K; New England Biolabs), anti-$(His)_6$ polyclonal antibody (His-probe; Santa Cruz), anti-Rac1 (23A8; Upstate) and Cdc42 (clone 44; BD Transduction Laboratories) were used.

2.3. Immunofluorescent analysis

C2C12-affixin cells seeded on coverslips were fixed for 15 min in 2% paraformaldehyde in PBS and then permeabilized for 10 min in 0.1% Triton X-100 in PBS. For double immunolabeling with anti-affixin and anti-dysferlin antibodies, cells were fixed at −20 °C for 10 min in 100% methanol. Coverslips were blocked with 5% goat serum–2% BSA in PBS and then incubated with primary antibodies for double labelling. Immunolabeling was detected with goat anti-rabbit IgG conjugated to FITC and goat anti-mouse IgG conjugated to Cy3 antibodies (Jackson Immunoresearch Laboratories). Cells were observed with a confocal laser-scanning microscope (LSM5 PASCAL, Carl Zeiss).

2.4. Immunoprecipitation assay

C2C12 and C2C12-affixin cells were lysed in 50 mM Tris–HCl, pH 7.5, 150 mM NaCl, 1 mM EDTA, 1% NP-40 and Complete (Roche). The lysates precleared with Protein A/G-agarose (ImmunoPure, PIERCE) were incubated with anti-affixin, αPIX and βPIX polyclonal antibodies and then Protein A/G-agarose was added before an additional incubation. Immunoprecipitated proteins were dissociated from beads by boiling in sample buffer and resolved by SDS–PAGE. Immunoblotting was performed as previously described [14].

COS-7 cells were co-transfected with T7-tagged wild type or deletion mutant human affixin (RP1 and RP2) and HA-tagged human βPIX using FuGENE 6 (Roche), and lysed for immunoprecipitation after 48 h. Affixin deletion mutants were generated as previously described [2,6]. Human βPIX cDNA was cloned from KIAA0142 gifted by Dr. T. Nagase (Kazusa DNA Research Institute, Japan). Immunoprecipitation was performed as outlined above except that anti-T7 (Novagen) and anti-HA (New England BioLabs) antibodies were used.

2.5. Gulutathione S-transferase (GST)-βPIX pulldown assay

The GST-βPIX proteins used for the pulldown assay were as follows: GST-SH3 (corresponding to amino acids of human βPIX 6-65), GST-Dbl-homology (DH) (aa 93–273), GST-pleckstrin-homology (PH) (aa 295–400), GST-CC (aa 586–638). cDNA fragments of these domains were amplified by PCR and subcloned into pGEX-5X-3 (GE Healthcare). GST fusion proteins expressed in BL21 were purified and bound to glutathione Sepharose 4B (GE Healthcare). The COS-7 cells overexpressing T7-tagged human affixin were lysed in the same lysis buffer used for immunoprecipitation. Precleared lysates were diluted with Buffer A (10 mM Tris–HCl, pH 8.0 and 0.1% Tween20) [15] and incubated with fusion protein bound to glutathione Sepharose 4B. After five washes in PBS, sample buffer was added to the beads and boiled for 5 min. Bound proteins were resolved by SDS–PAGE and subjected to immunoblotting using anti-T7 polyclonal antibody.

2.6. $(His)_6$-tagged affixin pulldown assay

cDNAs of deletion mutant affixin (RP1 and RP2) were amplified by PCR and subcloned into pET32a (Novagen). The $(His)_6$-tagged RP1 and RP2 were expressed in BL21DE3pLys(S), purified using Ni-NTA Spin kit (QIAGEN) and dialyzed against PBS. The pulldown assay using GST-βPIX fusion proteins and $(His)_6$-tagged RP1 or RP2 was performed as above.

2.7. Small GTPase activation assay

C2C12 and C2C12-affixin cells were grown until 60–70% confluence. Cells were lysed in 25 mM HEPES, pH 7.5, 150 mM NaCl, 1% Igepal CA-630, 10 mM $MgCl_2$, 1 mM EDTA and 2% glycerol. Lysates were incubated with glutathione Sepharose 4B conjugated with GST-p21-binding (CRIB) domain (residues 67–150) of human PAK-1 [16]. After three washes in the lysis buffer, the beads were resuspended in sample buffer and boiled for five minutes. Bound Rac1 and Cdc42 were separated on SDS–PAGE and subjected to immunoblotting.

2.8. Introduction of dominant-negative PIX into C2C12-affixin cells

Double mutation of βPIX (L238R, L239S) was introduced by PCR using appropriate internal primers. These two leucine residues were highly conserved among Dbl family member and shown to be essential for GEF activity [17]. βPIX and mutant βPIX (L238R, L239S) were subcloned into pSRD4-HA for transient expression. The constructs for transient expression of wild type αPIX and dominant negative αPIX (L383R, L384S) were as previously described [6]. C2C12-affixin cells were transfected with wild type or mutant PIX using Lipofectamine 2000. After 48 h, cells were fixed and immunolabeled as above.

3. Results

3.1. Immunofluorescent analysis of the C2C12-affixin cells

To investigate the possible role of affixin in skeletal muscle, stable C2C12 cell lines constitutively expressing T7-tagged human affixin were established. Expression of T7-tagged human affixin in C2C12-affixin cells was confirmed by immunoblot using anti-T7 antibody (Fig. 2). The expression level of total

affixin of C2C12-affixin cells was slightly higher than original C2C12 cell on immunoblotting using anti-affixin antibody (data not shown). Exogenous expression of T7-affixin in the C2C12 cells induced lamellipodia (Fig. 1). Only 10–20% of original C2C12 myoblasts showed lamellipodium formation, while more than half of the C2C12-affixin cells formed lamellipodia without any stimulation (Fig. 1). Formation of lamellipodia was confirmed by labelling F-actin with rhodamine–phalloidin.

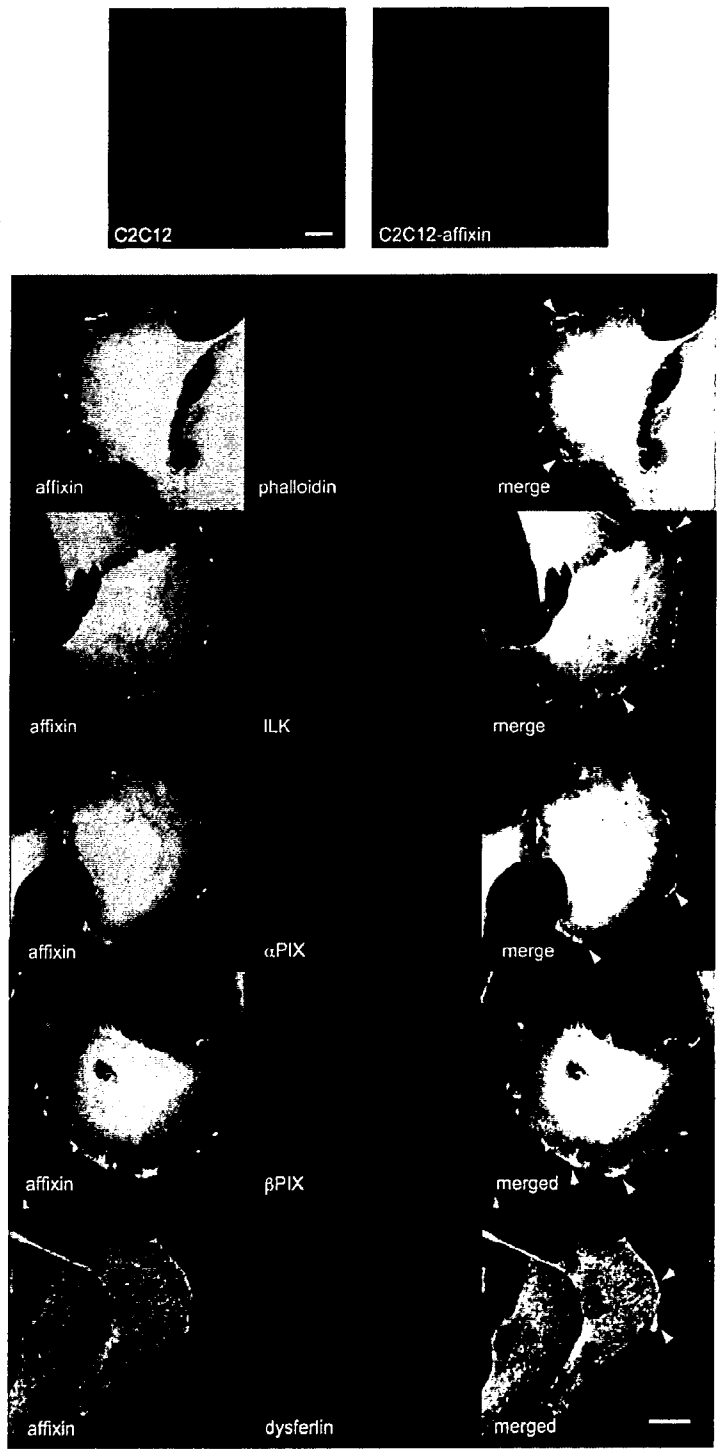

Fig. 1. Immunofluorescence analysis of stable C2C12 cells expressing human affixin. Lamellipodium formation was confirmed by rhodamine–phalloidin labelling. Antibodies were applied in five double-staining combinations: anti-affixin and phalloidin; anti-affixin and ILK; anti-T7 and αPIX; anti-affixin and βPIX and anti-affixin and dysferlin. Exogenous affixin was labelled with anti-T7 monoclonal antibody. Affixin co-localizes with ILK, αPIX, βPIX and dysferlin lamellipodium tips (arrowheads) in the C2C12-affixin cells. Scale bar, 20 μm.

As shown in Fig. 1, affixin accumulated and co-localized with F-actin at the tips of lamellipodia (Fig. 1). Transient expression of affixin without T7-tag promoted the lamellipodium formation of C2C12 cells as T7-tagged affixin (data not shown). Exogenous affixin was expressed in both the cytoplasm and at the tips of lamellipodia as C2C12-endogenous affixin (data not shown). We have previously shown the co-localization of affixin and ILK, a binding partner of affixin, at focal adhesion and at the tips of leading edge in Chinese hamster ovary (CHO) cells [2], and at sarcolemma of human skeletal muscle fibers [8]. In C2C12-affixin cells, ILK was enriched and co-localized with affixin in lamellipodia (Fig. 1) as original C2C12 cells. Cytoplasmic affixin in the C2C12-affixin cells was partially co-localized with ILK.

αPIX, a binding partner of affixin co-localizes with exogenous affixin at the tips of lamellipodia in 3Y1 cells (rat fibroblasts) [6] and CHO-K1 cells [18]. In the C2C12-affixin cells, endogenous αPIX accumulated intensely at the tips lamellipodia and co-localized with affixin (Fig. 1), while diffuse fine cytoplasmic granular staining of αPIX without lammellipodium accumulation was observed in the original C2C12 cells (data not shown). The C2C12-affixin cells also showed intense staining of βPIX, a homolog and a binding partner of αPIX [18,19], at lamellipodia, suggesting a possible association of affixin and βPIX. The co-localization of βPIX and affixin was observed at lamellipodia of original C2C12 cells (data not shown). Cytoplasmic α and βPIXs were also co-localized with affixin in the C2C12 cells. We then examined subcellular localization of dysferlin, a binding partner of affixin, in C2C12-affixin cells. As we reported earlier, cytoplasmic granular staining of dysferlin with no sarcolemmal accumulation was observed in the undifferentiated C2C12 cells [8]. In the C2C12-affixin cells, dysferlin accumulated and co-localized with affixin at lamellipodia. These results show that affixin co-localizes with ILK, αPIX, βPIX and dysferlin at the tips lamellipodia in the C2C12-affixin cells.

3.2. Analysis of the association between affixin and βPIX by coimmunoprecipitation assay

To define possible association between affixin and βPIX, immunoprecipitation was performed using the C2C12-affixin and original C2C12 cells. As shown in Fig. 2A, affixin was specifically co-immunoprecipitated with anti-βPIX antibody and reciprocally, βPIX was specifically co-immunoprecipitated by anti-affixin antibody in both C2C12-affixin and original C2C12 cells. There is no significant quantitative difference in co-immunoprecipitated affixin, α and βPIXs between C2C12-affixin and original C2C12 cells. Further, αPIX was specifically co-immunoprecipitated by anti-affixin [6] and anti-βPIX [18,19] antibodies in C2C12-affixin and original C2C12 cells as previously reported. Affixin or βPIX was not co-immunoprecipitated by control rabbit IgG.

To identify the region within affixin that interacts with βPIX, immunoprecipitation was also performed using COS-7 cells transiently co-transfected with full-length or deletion mutants [2] of T7-human affixin (Fig. 2A) and HA-human βPIX. As shown in Fig. 2B, the full-length T7-affixin was co-immunoprecipitated by anti-HA antibody. Reciprocally, HA-βPIX was specifically co-immunoprecipitated by anti-T7 antibody, while control mouse IgG was not. Affixin-RP1 containing N-terminal CH domain (CH1) was co-immunoprecipitated by

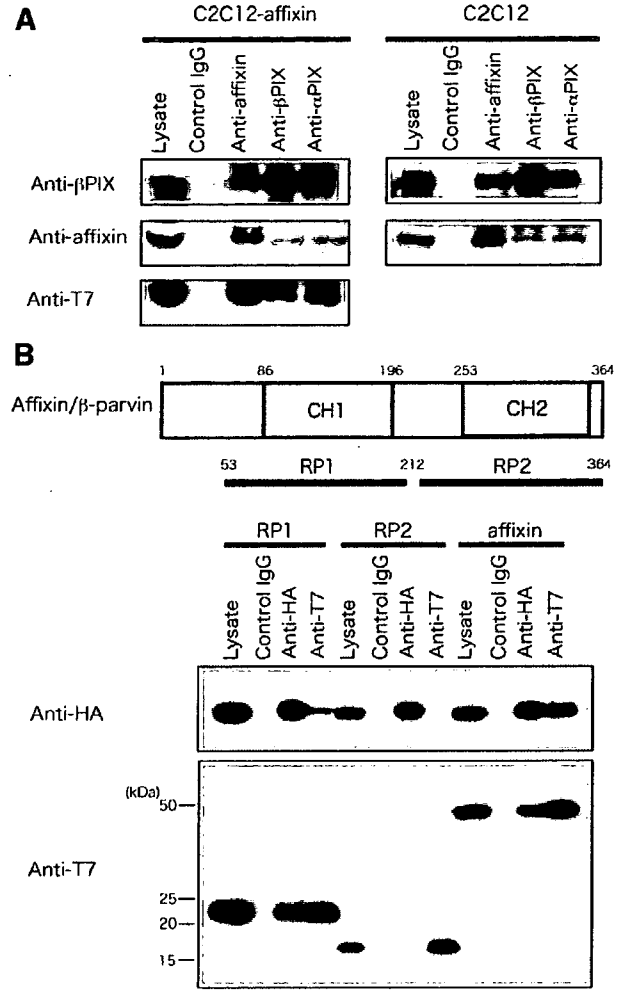

Fig. 2. (A) Confirmation of the association of affixin and βPIX. Cell lysates form the C2C12-affixin and C2C12 cells were immunoprecipitated with anti-affixin, anti-βPIX and anti-αPIX antibodies. Immunoprecipitates were subjected to immunoblotting with the same antibodies used for immunoprecipitation. Affixin was specifically co-immunoprecipitated by anti-βPIX antibody and *vice versa*. Co-immunoprecipitation of T7-tagged exogenous affixin was confirmed by probing with anti-T7 antibody. As reported previously, αPIX was specifically co-immunoprecipitated by anti-affixin and anti-βPIX antibodies. (B) Identification of βPIX-binding domain of affixin by immunoprecipitation assay. T7-tagged wild type or deletion mutants of affixin and HA-tagged βPIX were co-expressed in COS-7 cells. A schema of deletion mutants of affixin is shown at the top. Immunoprecipitation was performed with anti-T7 and anti-HA antibodies. βPIX was co-immunoprecipitated with wild type affixin and RP1 and *vice versa*, but not with RP2.

HA-βPIX (Fig. 2B), while affixin-RP2 containing C-terminal CH domain (CH2) was not. These and previous reported findings [6] suggest that affixin can interact with both α and βPIXs via CH1 domain.

3.3. Identification of the binding domain of βPIX to affixin by pulldown assay

To identify affixin-binding domain of βPIX, a pulldown assay was performed. The lysates from COS-7 cells overexpress-